Bedrock landsliding, river incision, and transience of geomorphic hillslope-channel coupling: Evidence from inner gorges in the Swiss Alps

Oliver Korup[1] and Fritz Schlunegger[2]

Received 7 October 2006; revised 18 May 2007; accepted 18 June 2007; published 27 September 2007.

[1] The formation of inner gorges cut into bedrock has been explained as relief rejuvenation by fluvial incision in response to rapid base level drop, repeated glaciations, frequent pore pressure–driven landsliding focused at hillslope toes, or catastrophic outburst flows from natural dam failures. Prominent inner gorges occur in soft Mesozoic Bündner schist and lower Tertiary flysch units of the formerly glaciated Alpenrhein catchment, eastern Swiss Alps. Their channel and hillslope morphologies differ from basins characterized by strong glacial or landslide imprints, while formally resembling the theoretically predicted transient response of detachment-limited bedrock rivers to rapid base level fall by headward knickpoint migration. Assuming a postglacial onset of fluvial bedrock incision into a Last Glacial Maximum surface in response to base level drop induced by downwasting of trunk valley glaciers requires downcutting rates $E > 20$ mm yr^{-1} and requires hillslopes to adjust by frequent landsliding toward development of a threshold state. We test this scenario using data on surface uplift, geomorphometry, geomorphic hillslope coupling, and probabilistic slope stability models. We find that adjustment of inner gorge walls through landsliding is mainly strength limited and structurally controlled, and threshold conditions are restricted to the lower 25% of local hillslope relief. Mass movement processes on upper hillslopes remain largely decoupled from channel incision despite inferred postglacial specific sediment yields of 10^4 m^3 km^{-2} yr^{-1} from the studied basins. Conversely, several constraints imposed by fluvial bedrock detachment, postglacial sediment yields, and bedrock landsliding argue for a pre-Holocene origin for at least some of the inner gorges in the area. This implies partial protection of fluvial gorge topography by subglacial sediment fill during the last (Würm) extensive glaciation and implies that glaciers were insufficient to fully eradicate fluvially sculpted bedrock topography. This leads us to conclude that lithology and major climate oscillations should be considered as further alternative controls on inner gorge formation.

Citation: Korup, O., and F. Schlunegger (2007), Bedrock landsliding, river incision, and transience of geomorphic hillslope-channel coupling: Evidence from inner gorges in the Swiss Alps, *J. Geophys. Res.*, *112*, F03027, doi:10.1029/2006JF000710.

1. Introduction

[2] Inner gorges are landform elements that form at the interface between hillslopes and river channels. They are characterized by a convex break in hillslope gradient, and lined, often symmetrically, by hillslope toes significantly steeper than those of upper valley flanks [*Kelsey*, 1988]. This distinctive "valley-in-valley" topography [*Baillie and Norbu*, 2004] may occur in bedrock or debris slopes alike. There are at least four processes that favor the formation of inner gorges: (1) relief rejuvenation by fluvial incision in response to rapid base level drop [*Ahnert*, 1988; *Densmore et al.*, 1997; *Bonnet et al.*, 2001; *Stock et al.*, 2005]; (2) repeated glaciations of differing erosion potential [*Mitchell et al.*, 1999]; (3) frequent pore pressure-driven landsliding that preferentially undermines hillslope toes [*Kelsey*, 1988; *Densmore and Hovius*, 2000]; and (4) catastrophic and highly erosive outburst flows from natural dam failures [*Knudsen and Marren*, 2002; *Rudoy*, 2002]. Despite these different mechanisms of formation and their possible superposition, inner gorges are commonly interpreted as transient landforms of relief rejuvenation [e.g., *Whipple et al.*, 2000], which may be eventually be removed by slope-clearing landslides [*Densmore et al.*, 1997]. The age of an inner gorge may thus record a marked change in process rates of both hillslope and channel systems [*Stock et al.*, 2005]. However, the rates of geomorphic coupling, simply regarded here as the exchange of mass and energy, between

[1]Research Unit Avalanches, Debris Flows and Rockfalls, Swiss Federal Research Institute for Forest, Snow and Landscape Research, Davos, Switzerland.
[2]Institute of Geology, University of Berne, Berne, Switzerland.

0148-0227/07/2006JF000710

hillslopes and channels, are rarely quantified [*Schlunegger et al.*, 2002], although recent modeling advances have been made for soil-mantled landscapes [*Mudd and Furbish*, 2005]. Persisting research gaps for bedrock-dominated landscapes derive from the many unknowns of how sudden rate changes in bedrock channel incision are communicated to hillslope systems. In tectonically active mountain belts, for instance, frequent landsliding on threshold hillslopes is one of the purported means of relief adjustment to fluvial bedrock incision [*Burbank et al.*, 1996]. However, the preservation of continuous inner gorges, slot canyons, or high-level bedrock strath terraces in these areas is seemingly at odds with the notion of hillslope gradients being maintained by, albeit spatially variable, threshold landsliding. This is because, although these landforms attest to efficient fluvial incision, they also document the limited response of hillslopes to this process [*Tinkler and Wohl*, 1998]. Obviously, rock mass properties, which can be subsumed as strength and incision limits to hillslope stability and relief [*Schmidt and Montgomery*, 1995], become important controls on dictating the rates of local hillslope relief adjustment to channel processes.

[3] Impressive inner gorges occur in many parts of the European Alps, where they, beheld intuitively, resemble landforms of both rejuvenation and high process activity, though little is known about their ages or the geomorphic processes that formed them. This motivates an enquiry on the underlying causes of and controls on their formation, which we wish to elucidate in a study area of the eastern Swiss Alps as a simple field test of previously proposed models [e.g., *Kelsey*, 1988; *Densmore et al.*, 1997]. More specifically, our objective is to use the combined results from field observations, geomorphometry, surface uplift data, and probabilistic slope stability modeling to derive first-order quantitative constraints on the dominant processes, rates, and timing of gorge incision with respect to glacial-interglacial cycles during the Quaternary. In the first part of this paper, we present results from a morphometric analysis that we augment with geomorphic field evidence to bracket the time of inception and rates of inner gorge incision in the study area. In the second part, we use a simplistic slope stability model to probabilistically test for the likelihood of threshold-landsliding and lithological controls of inner gorge cutting. We build the discussion of our results around two contrasting scenarios, which argue for either a postglacial or a pre-Holocene onset of gorge cutting, and conclude with several implications of fluvial relief inheritance and rejuvenation for models of inner gorge formation.

2. Study Area

[4] Major continuous bedrock gorges occupy >10% of the channel network of the Alpenrhein catchment in eastern Switzerland, which drains 4470 km^2 above the town of Sargans (Figure 1a). The exact proportion is likely to be much higher, but difficult to assess, partly because many gorges were infilled by reservoirs for hydropower generation. The regional geology comprises a broad range of rock types with marked differences in erodibility [*Kühni and Pfiffner*, 2001]. The northern parts are made up of crystalline basement covered by metasediments of the European continental plate, which are overlain by a stack of Penninic and Austroalpine nappes that partly originated from the African continental plate. The Penninic nappes (Figure 1b) comprise high-grade basement rocks and a medium- to low-grade metasedimentary cover, encompassing a suite of metacarbonates and highly erodible shales and arenites several thousands of meters thick, including the Bündner (calc-)schists and flysch units [*Kühni and Pfiffner*, 2001]. In the southeast, the Austroalpine units are composed of a sequence of basement rocks covered by Mesozoic carbonates.

[5] The Alpenrhein was covered by an extensive ice stream network as part of the 1.6×10^4 km^2 Rhine-Linth glacier during the last (=Würm) glaciation, which in trunk valleys has caused glacial overdeepening roughly down to sea level [*Persaud and Pfiffner*, 2004]. Only the highest peaks remained as nunatakker. Locally, hillslopes are mantled by glacial tills several tens of meters thick, and many of the major valley trains host postglacial sediment fills several hundreds of meters thick [*Hinderer*, 2001]. Impressive inner gorges with local relief of >100 m occur in many trunk and tributary basins (Figures 2 and 3). They predominantly occur in soft Cretaceous Bündner schist and lower Tertiary flysch lithology. The Bündner schists mainly comprise calc-schists of highly varying degrees of metamorphism. They are interbedded with shales and quartzites, and lithologically similar to the younger flysch deposits [*Bousquet et al.*, 1998]. Both rock types are strongly folded with inclusions of sheared and broken shale and sandstone layers containing variable amounts of swelling clay minerals, and weather rapidly to produce platy to flaky fragments [*Huder*, 1976], which in places can readily be dislodged from outcrops by hand. Gorges of comparable size occur in other calcareous and dolomitic rocks, while they are less frequent and less prominently incised in harder crystalline rocks of, e.g., the Silvretta nappe (Figure 1b). The dendritic network and sinuosity of the gorges excludes any preferential incision along tectonic fault zones or other lineaments of low rock mass strength. Contemporary rates of surface uplift measured by geodetic surveys of first-order leveling benchmarks relative to the benchmark at Aarburg between ~1905 and 1990 contain effects of postcollisional exhumation and isostatic rebound, and amount to U_h = 0.8–1.4 mm yr^{-1} [*Kahle et al.*, 1997] (Figure 1c). The study area has also experienced some of the highest exhumation rates in the Alps in the recent geological past as indicated by apatite fission track ages <5 Ma [*Schlunegger and Willett*, 1999].

[6] To quantify our initial qualitative observations of differing drainage basin response in general, and the geomorphic properties of basins featuring inner gorges in particular, we conducted a morphometric analysis of 28 basins with catchment areas $3 < A < 20$ km^2 (Figure 1 and Table 1). We focused on small tributary basins to capture bedrock channel morphologies on the assumption of short response times to tectonic or climatic forcing or other forms of intrinsic transience, such as significant changes to sediment flux [*Schlunegger et al.*, 2002]. At least three general types of drainage basin morphologies can be distinguished by visual inspection: (1) glacial trough basins featuring characteristic u-shaped cross sections, mostly deglaciated cirques, patchy moraine cover, rock knobs and steps, hanging valley outlets drained by minor

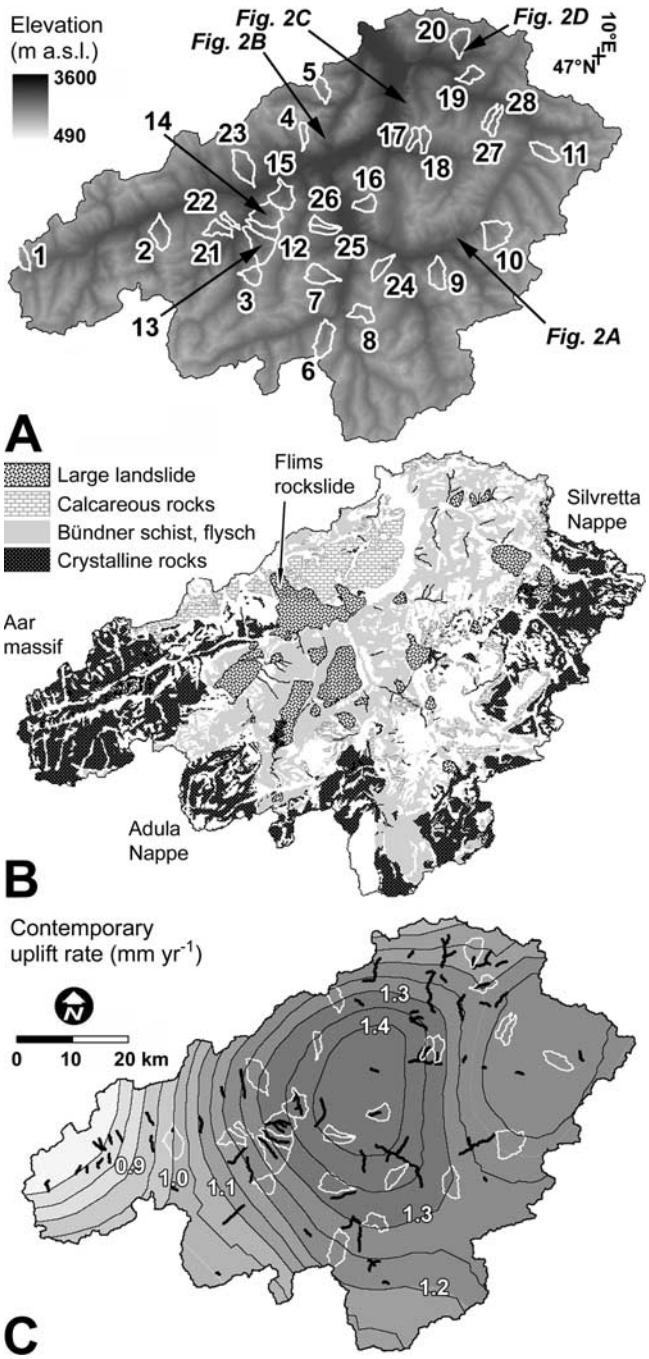

Figure 1. (a) Topography of Alpenrhein catchment and locations of the 28 study basins (drainage divides in white; numbers refer to Table 1). (b) Dominant rock types and selected large (>1 km^2) landslides. White patches denote both sedimentary cover and minor lithologic variations. (c) Contemporary rates of surface uplift U_h measured by geodetic surveys [*Kahle et al.*, 1997]. Major bedrock gorges are shown as black lines.

gorges or waterfalls, and generally little postglacial fluvial modification; (2) basins perched on top of large, deep-seated, and slow-moving landslides of the sackung type, involving the gradual collapse of valley flanks on a 10^1-km^2 scale; and (3) basins that show typical glacially smoothed features above steep and deeply (>100 m) incised v-shaped inner bedrock gorges that flank most of the channels (Figure 2). The concurrence of these basin-scale morphological differences clearly points to transient landscape conditions with respect to geological time.

3. Methods and Assumptions

[7] We used a 25-m DEM to compute a range of hillslope and channel metrics that are commonly employed to infer process relationships in tectonic geomorphology. From slope area regression we obtained the indices of concavity θ_c and steepness k_c for bedrock channels [*Whipple and Tucker*, 2002]. We used k_c, fixed for a concavity $\theta_{c'} = 0.45$, as a proxy for specific stream power or, more generally, fluvial erosion potential for comparison between channels of differing θ_c [e.g., *Safran et al.*, 2005; *Korup*, 2006]. We adapted this approach for computing hillslope steepness k_h corrected for the effects of catchment position, for all cells with contributing areas smaller than the channelization threshold A_{ch} determined from high-resolution orthophotos and fieldwork, and using the regional mean of $\theta_{h'} = 0.07$ as

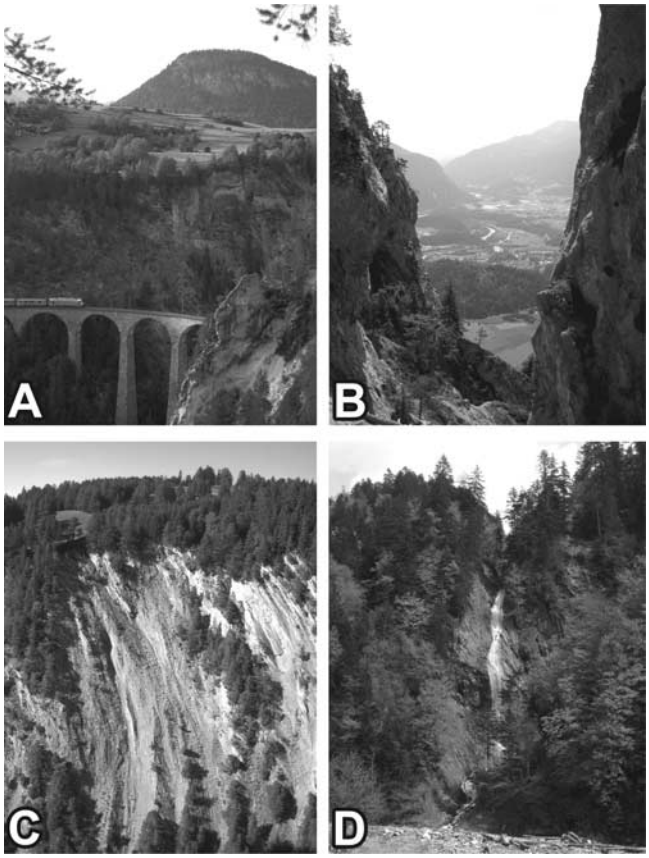

Figure 2. Inner gorges cut in noncrystalline rocks of the Alpenrhein catchment (for locations, see Figure 1a). (a) Zügenschlucht: dolomites (note train for scale). (b) Bedrock gorge truncated in its lower reaches by giant (10^9 m^3) postglacial rockslide in carbonate, Tamins near Flims. (c) Detail of gorge wall with well-defined cliff edge, Hagtobel (Bündner schist and thin colluvial cover). (d) Gorge wall detail with waterfall at hanging tributary mouth (Bündner schist).

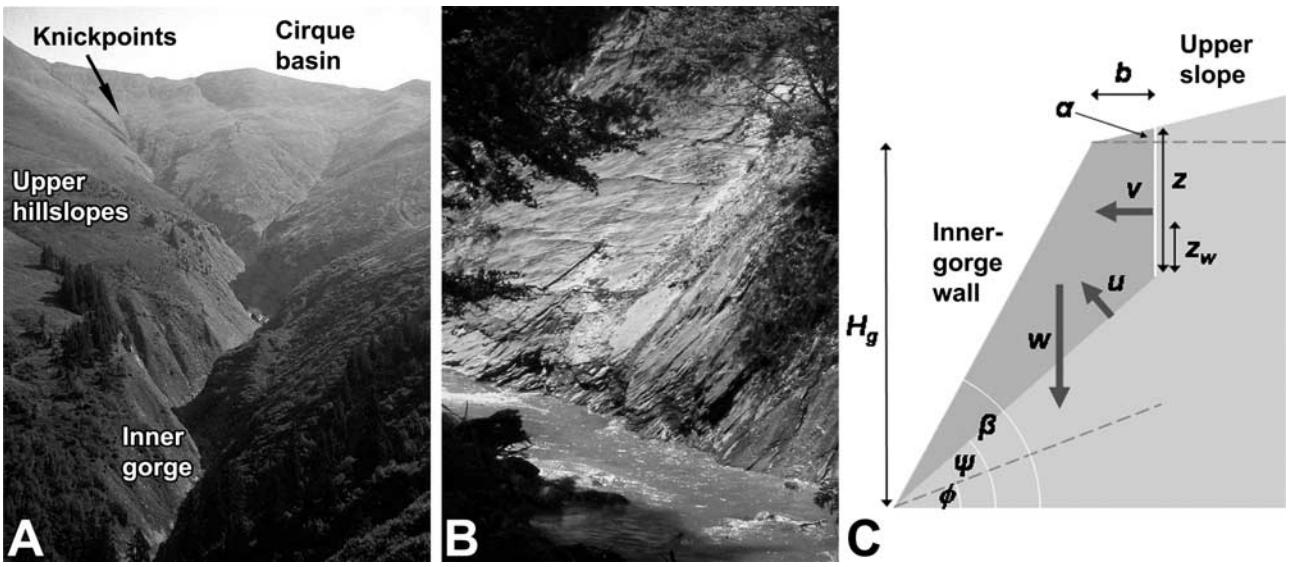

Figure 3. (a) Inner gorge of basin 12, extending up into headwaters. (b) Bedrock channel undercutting dip slope in Bündner schist, with lateral bedrock detachment facilitated by wedge failure. (c) Sketch of inner gorge wall showing parameters used for limit-equilibrium analysis of planar rock slope stability. See text for explanation.

a reference. To characterize the relationship between channel and hillslope morphology for each basin, we defined a dimensionless concavity ratio,

$$R_\theta = \frac{\theta_c}{\theta_h}. \tag{1}$$

We expect high values of R_θ to indicate concave channels bounded by rectilinear hillslopes, whereas low or negative values should characterize convex channels with more concave hillslopes.

[8] To further identify the inner gorges at the basin scale, we adapted the method of relating local hillslope gradient S_h to normalized hillslope position x_s [*Densmore and Hovius*, 2000],

$$x_s = \frac{x_d}{x_d + x_u}, \tag{2}$$

where x_d and x_u are the distances from each cell to the local channel and hillcrest, respectively. For bins of width Δx_s = 0.05, we calculated the probability density

$$P(a) = P(S_h \geq S_a), \tag{3}$$

where S_a is an arbitrary slope gradient, for which we appointed values of 0.47, 0.58, 0.70, and 1, i.e., 25°, 30°, 35°, 40°, and 45°, respectively. Here, we use the relative deviation from the mean $\langle P(a) \rangle$,

$$P(a)^* = \frac{P(a) - \langle P(a) \rangle}{\langle P(a) \rangle}, \tag{4}$$

to assess trends in the probability of encountering steep gradients at a given hillslope position.

[9] The extent of inner gorges was mapped for each basin (Figure 1), and complemented by measurements from other basins not studied in further detail; the heights and mean slope gradients of the gorge walls, H_g and $\langle S \rangle$, were manually recorded at each intersection of the 20-m contours with the valley bottom, and complemented by local measurements of A and k_c. We did not sample at tributary junctions or where the upper edges of the gorges were found to be poorly defined. In order to quantify the volume of material eroded from the inner gorges, V_e, we used a tension spline (TS) interpolation between elevation points recorded at their upper edges. The resulting artificial surfaces do not necessarily represent any actual past geomorphic surfaces. By subtracting the present-day topography from these model surfaces, however, we obtain first-order estimates of V_e for each basin, assuming that none of the gorges are structural in origin.

4. Morphometric Characteristics of Inner Gorges

4.1. Basin Types

[10] The distribution of eight basin-averaged terrain variables stratified by basin type show different characteristic ranges. We find that glacial basins have the highest mean basin elevation $\langle E \rangle$ (Figure 4), whereas the basins perched on top of large landslides have the lowest relief, as their channels often drain only the lower parts of hillslopes. Basins with inner gorges have the lowest values of the hypsometric integral, but are also have the steepest slopes on average. Their hillslopes tend to be the most rectilinear (mean θ_h = 0.04), and stand out against the more concave glacial basins (Figure 4). Basins with inner gorges also have the highest values of R_θ = 12.9, whereas basins without inner gorges are characterized by a negative R_θ. On average, channels appear to be steepest in glacial basins, although much of this effect needs to be attributed to convex long profiles with a large degree of glacial landform inheritance. In summary, however, we find that these differences in the

Table 1. Hillslope and Channel Metrics Stratified by Basin Type, Alpenrhein Catchment, Swiss Alps[a]

		Basin		Hillslopes			Channels					
Basin	Name	A, km^2	H, km	$\theta_h(\pm\sigma)$	k_h, km$^{0.14}$	R^2	$\theta_c(\pm\sigma)$	k_c, km$^{0.9}$	R^2	A_{ch}, km	Main Lithology[b]	Related Knickpoints[c]
						Glacial						
1	Val Val	6.5	1.4	0.08 ± 0.004	0.42	0.98	−0.63 ± 0.09	0.49	0.02	0.1	gn, sch	~
2	Zavragia	12.9	1.9	0.05 ± 0.01	0.40	0.86	0.44 ± 0.05	0.59	0.22	1.0	gn, sch	N
3	Grava	8.2	1.7	0.08 ± 0.01	0.41	0.90	−0.77 ± 0.10	0.93	0.01	0.2	cas, ph, bt	Y
4	Trimosa	4.4	1.9	0.18 ± 0.02	0.32	0.78	−1.92 ± 0.19	1.07	0.25	0.6	cu	N
5	Tersol	8.2	1.6	0.11 ± 0.01	0.48	0.97	−0.47 ± 0.06	0.60	0.13	0.1	cas, ph	Y
6	Suretta	15.1	1.7	0.09 ± 0.004	0.42	0.97	0.54 ± 0.06	0.49	0.21	0.3	gn, seds	~
7	Donath	12.6	2.0	0.07 ± 0.01	0.29	0.82	0.39 ± 0.05	0.53	0.05	0.6	cu	Y
8	Lambegn	8.5	1.6	0.12 ± 0.01	0.32	0.86	−0.89 ± 0.10	0.80	0.21	0.3	do, ca	N
9	Schaftobel	12.3	2.1	0.15 ± 0.02	0.43	0.85	−0.92 ± 0.11	0.75	0.01	1.8	do, ca	Y
10	Inneralp	19.2	1.6	0.09 ± 0.01	0.38	0.91	0.33 ± 0.03	0.38	0.44	0.1	gn, do	N
11	Mönchalp	9.8	1.5	0.07 ± 0.01	0.38	0.86	0.73 ± 0.09	0.62	0.01	0.1	gn	N
						Inner Gorges						
12	Pitasch	10.3	2.0	0.03 ± 0.003	0.48	0.87	0.50 ± 0.04	0.44	0.48	0.4	ca	N
13	Duvin	19.7	2.0	0.01 ± 0.004	0.55	0.06	0.58 ± 0.04	0.45	0.72	0.4	ca	N
14	Riein	17.9	2.1	0.06 ± 0.01	0.46	0.83	0.56 ± 0.03	0.52	0.69	0.1	ca	N
15	Bruen	14.3	1.9	0.05 ± 0.01	0.48	0.70	0.59 ± 0.04	0.44	0.65	0.15	ca	Y
16	Almen	8.1	1.7	0.03 ± 0.01	0.52	0.63	0.43 ± 0.04	0.50	0.51	0.2	ca, cas, ph	N
17	Castiel	4.9	1.7	0.03 ± 0.01	0.43	0.59	0.52 ± 0.06	0.58	0.01	0.04	ca	N
18	Clasaurer	6.5	1.6	0.07 ± 0.01	0.34	0.94	0.45 ± 0.05	0.47	0.00	0.1	ca, cas, ph	N
19	Buchner	7.6	1.4	0.05 ± 0.005	0.38	0.91	0.40 ± 0.02	0.32	0.89	0.2	ca	N
20	Salgina	11.4	1.6	0.04 ± 0.004	0.46	0.92	0.44 ± 0.04	0.36	0.57	0.3	ca	N
						Landslides						
21	Lumnez	8.0	1.4	0.05 ± 0.01	0.22	0.71	−0.57 ± 0.09	0.57	0.04	0.2	ls, ca	N
22	Vella	3.0	1.5	0.08 ± 0.01	0.23	0.74	−0.47 ± 0.07	0.32	0.05	0.1	ls, ca, cas, ph	N
23	Schluein	16.1	1.8	0.04 ± 0.004	0.27	0.86	0.40 ± 0.04	0.46	0.12	0.2	sch, ph	N
24	Stierva	7.6	1.8	0.07 ± 0.01	0.24	0.93	−0.86 ± 0.09	0.71	0.28	0.3	ls, cs, ph	~
25	Portein	4.5	1.4	0.03 ± 0.004	0.21	0.82	0.28 ± 0.04	0.29	0.01	0.1	cas, ph, ca	N
26	Malanotg	5.8	1.4	0.04 ± 0.004	0.21	0.88	0.27 ± 0.04	0.34	0.00	0.6	cas, ph	~
27	Casolf	5.8	1.4	0.08 ± 0.01	0.20	0.62	−0.88 ± 0.11	0.44	0.06	0.6	ls, cs, ph	~
28	Wissbach	4.9	1.5	0.07 ± 0.01	0.23	0.80	−0.46 ± 0.05	0.41	0.18	0.6	ls, cs, ph	~
Mean of 1–*28*		9.8 ± 4.7	1.7 ± 0.2	0.07 ± 0.04	0.36 ± 0.11	0.81 ± 0.18	−0.04 ± 0.68	0.53 ± 0.18	0.24 ± 0.27	0.33 ± 0.36	-	-
Mean of 12–20		11.2 ± 5.1	1.8 ± 0.2	0.04 ± 0.02	0.46 ± 0.06	0.72 ± 0.28	0.50 ± 0.07	0.45 ± 0.08	0.50 ± 0.31	0.22 ± 0.13	-	-
Mean of 1–11; 21–28		9.1 ± 4.5	1.6 ± 0.2	0.08 ± 0.04	0.32 ± 0.09	0.85 ± 0.01	−0.29 ± 0.70	0.57 ± 0.21	0.12 ± 0.12	0.39 ± 0.43	-	-

[a]Numbers in first column refer to Figure 1a.

[b]Here bt, biotite schist; ca, calcareous (Bündner schist); cas, calcareous schists; cu, calcaerous (undifferentiated); do, dolomites; gn, gneisses; ls, blocky landslide debris; ph, phyllites; sch, schist; sed, cover sediments.

[c]Tilde means knickpoint at major bedrock-sediment contact.

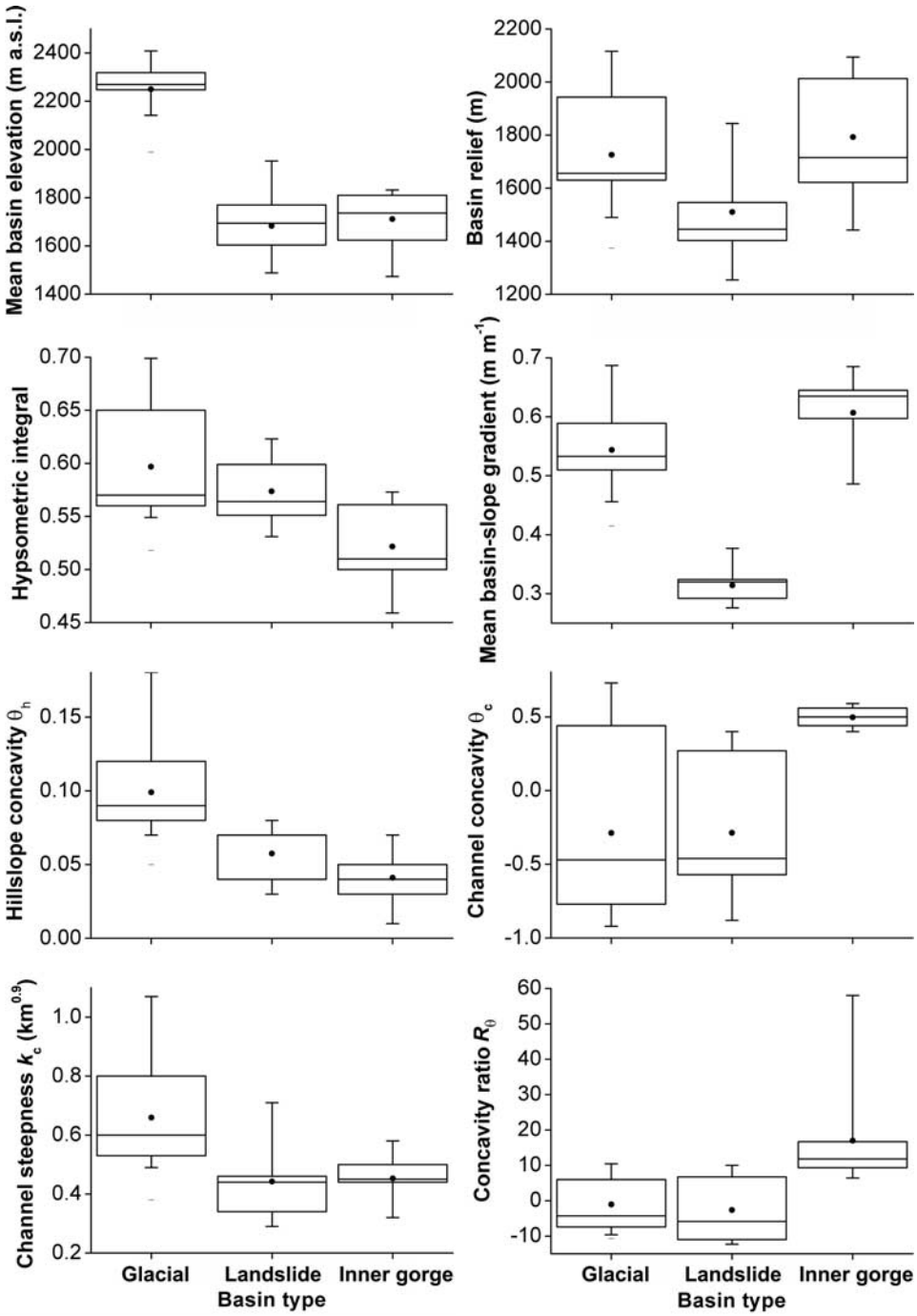

Figure 4. Box-and-whisker plots of selected morphometric properties stratified by basin type for basins in Table 2.

ranges of terrain variables formally support our initial qualitative distinction between three basin types.

4.2. Inner Gorge Channels

[11] The inner gorges in the study basins are characterized by steep ($\langle S_c \rangle > 0.16$) and deeply incised ($H_g > 50$ m) channels flanked by rectilinear and occasionally subvertical bedrock cliffs (Figures 2 and 5 and Table 2). In the basins studied, inner gorges extend over ~70% of the lower trunk channels (Figure 3a), and occupy the lower 25% of local hillslope relief, and 10% of total basin relief H, on average (Table 2). Some of the channel beds have an alluvial cover, especially in reaches with torrent control measures such as sediment retention basins, yet we find from high-resolution orthophotos that larger patches of valley floor sediment are absent. Long profiles show distinctive channel knickpoints, some of which form waterfalls, while channels above most knickpoints are bounded by more gentle banks and hillslopes. These bedrock knickpoints are only rarely related to major lithologic contacts (Figure 6 and Table 1). Most inner gorges extend up into major tributaries, locally via hanging outlets or bedrock slots of tributary ravines (Figure 2d). In

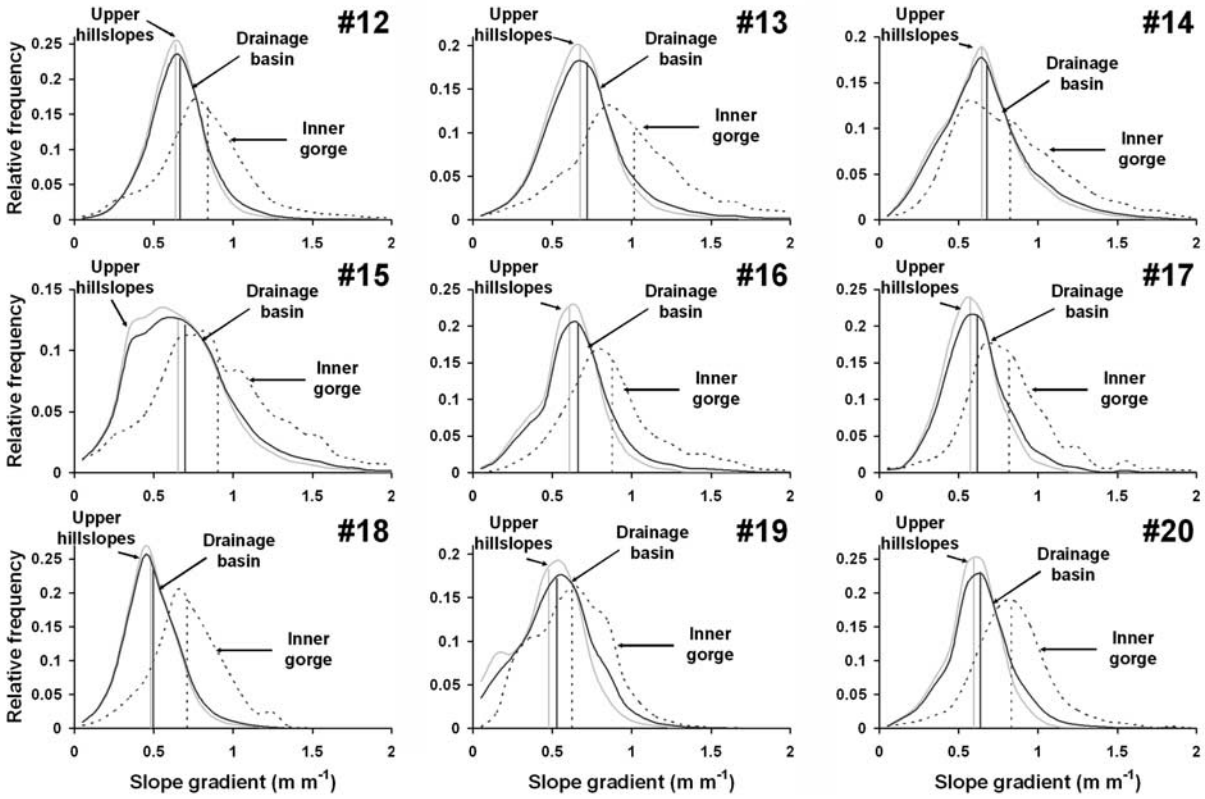

Figure 5. Area-normalized slope gradient histograms of basins with inner gorges (Table 2), stratified by upper hillslopes (gray curve), inner gorges (dashed curve), and the whole drainage basin (black curve). Vertical lines show mean values.

some headwaters, the gorges are linked to active dendritic gully networks. The upper edges of the inner gorges roughly mark concave long profiles similar to those of the modern river profiles (Figure 6). The profile of the upper edge of the inner gorge and the profile of the modern river appear to join at their upstream ends at major channel knickpoints, marked by the highest values of k_c along a given profile. Channel concavity in the inner gorges is well developed with a mean $\theta_c = 0.50$ (Table 1). In contrast, basins with pronounced glacial and landslide imprint have much more convex to straight channel long profiles (Figure 4). We find that the spatial pattern of channel steepness index k_c in basins with inner gorges is independent of that of short-term surface uplift rate U_h ($R^2 < 0.25$; Figure 7a). Similarly, no correlation can be observed with the pattern of long-term apatite fission track ages in the area [*Persaud and Pfiffner*, 2004].

4.3. Inner Gorge Hillslopes

[12] In catchments with inner gorges, distinctive convex hillslope knickzones define the upper edges of the gorge

Table 2. Morphometric Properties of Selected Inner Gorges in the Study Area

	Length of Inner Gorge			Mean Incision Depth		Area of Inner Gorge					
Basin	L_g, km	% of Total	Mean Channel Gradient $\langle S_c \rangle$	H_g ($\pm\sigma$)	% of H	A_g, km^2	% of Area	Upper Width, km	% Forest Cover	Volume Eroded[a] V_e, 10^6 m^3	Inferred Postglacial[b] Q_s, 10^3 m^3 km^{-2} yr^{-1}
12	7.1	88	0.273	88 ± 40	4 ± 2	1.5	15	0.11–0.40	57.0	51	2.3–3.4
13	3.8	69	0.210	169 ± 73	8 ± 4	2.8	14	0.10–0.66	42.8	171	4.1–6.1
14	4.6	64	0.174	154 ± 37	9 ± 2	3.1	17	0.21–0.66	53.3	107	2.3–3.4
15	4.4	64	0.168	168 ± 44	9 ± 2	2.4	17	0.19–0.60	61.9	108	3.0–4.5
16	4.5	91	0.395	206 ± 108	12 ± 6	1.6	20	0.15–1.12	63.0	65	2.7–4.0
17	2.9	53	0.443	117 ± 29	7 ± 2	0.9	18	0.12–0.53	56.0	21	1.5–2.3
18	3.9	64	0.300	79 ± 29	5 ± 2	0.4	6	0.12–0.42	97.9	11	1.9–2.8
19	>2.7	>50	0.186	316 ± 84	22 ± 6	2.7	36	0.44–1.73	74.8	200	4.9–7.4
20	4.6	72	0.190	205 ± 68	13 ± 4	2.1	18	0.18–0.74	62.2	83	2.6–3.9
Mean	4.3	68	0.260	167	10	1.9	18	0.18–0.76	63.2	91	2.8–4.2
σ	1.3	14	0.101	72	5	0.9	8	0.10–0.42	15.6	64	1.1–1.6

[a]Estimated using tension spline interpolation.
[b]Normalized by gorge area and assuming age of LGM surface of 15 and 10 ka, respectively.

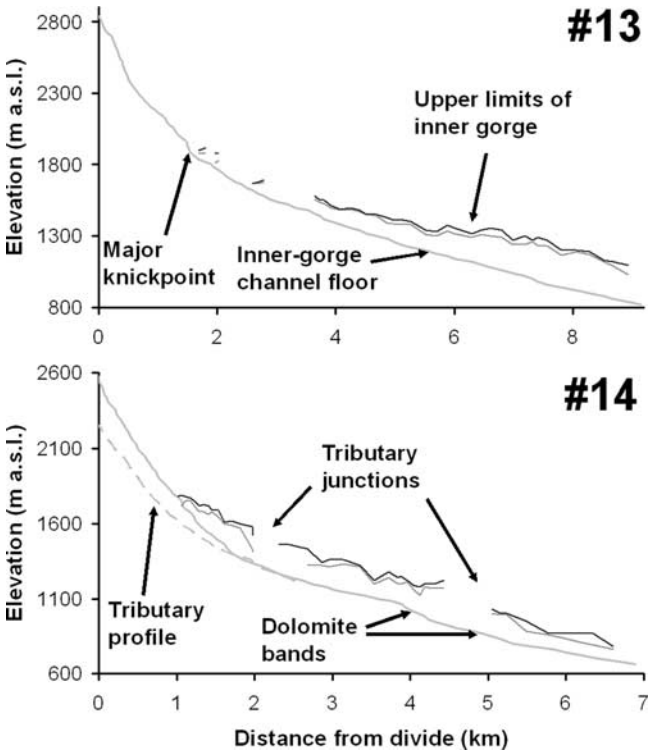

Figure 6. Long profiles of channels and upper edges of inner gorges (gray, minimum; black, maximum) for basins 13 and 14 (Table 1). Note merging of gorge ''treads'' and channels at channel knickpoints, which may be interpreted as the result of fluvial adjustment to rapid base level fall. Local exposures of dolomite spatially coincide with convex knickpoints.

walls, which are significantly steeper than the soil-mantled hillslopes of the upper basin (Figure 5). Field observations reveal that dry raveling, rockfall, topple and slide, debris flows, and gully erosion are the dominant processes of erosion of the gorge walls, which are on average ~60% forest covered (Figure 3b). However, geomorphic hillslope-channel coupling is limited to episodic slope failures along the gorge walls and to steep tributaries, which transfer sediment directly into the gorges [*Schlunegger et al.*, 2002]. In contrast, processes on upper slopes such as solifluction, gullying or shallow soil sliding are largely decoupled from trunk channel processes (Figure 3a). When averaged over a given catchment, the *average* incision depth of gorges is unrelated to both channel steepness k_c and drainage basin size A (Figures 7b and 7c), hence gorges appear to be prominent regardless of their catchment position. In individual basins, the local height of the gorge walls, H_g, increases with catchment area (Figure 8); that is, gorges become seemingly deeper downstream. Where alluvial cover is absent H_g can be used to estimate the total incision depth. The mean slope gradients of hillslopes and gorge walls vary little with A, and indicate the dominance of rectilinear slope profiles, which are slightly more concave for the gorge walls, while the spatial distribution of slope gradient with slope position varies considerably (Figure 9). Moreover, the data do not show any significant control of fluvial erosion potential, approximated by k_c, over H_g or $\langle S_h \rangle$ (Figure 8).

5. Geomorphic Constraints on the Formation of Inner Gorges

[13] The range of values of several geomorphic hillslope and channel metrics, i.e., mean elevation and slope gradient, basin relief, hypsometric integral, concavity and steepness, as well as concavity ratio, differ noticeably between the types of study basins (Figure 4), and quantitatively support earlier notions of transient landscape conditions in the eastern Swiss Alps [e.g., *Schlunegger and Hinderer*, 2003]. Similar results were presented by *Brardinoni and Hassan* [2006] for the postglacial landscape of coastal British Columbia. Our main interest here, however, is the limited geomorphic coupling of hillslope with channel processes in the basins with inner gorges (Figures 4, 5, 7, and 8). In the following, we augment our morphometric results with several other independent lines of geomorphic evidence to further explore the role of inner gorges within the postglacial landscape disequilibrium.

5.1. Fluvial Detachment of Bedrock

[14] The river long-profile geometries of many of the studied inner gorges formally resemble the transient response of bedrock channels to base level fall by headward knickpoint migration [*Whipple and Tucker*, 2002], assuming that the upper edges of the gorges aptly record the geomorphic surface before downcutting commenced (Figure 6). The continuity of the inner gorges along trunk and tributary channels points to a propagating, and not a randomly distributed, adjustment process. Importantly, the concavity of the gorge channels is well defined and close to $\theta_c = 0.45$, a value typically observed for bedrock rivers in mountain belts (Table 1). This attests to a strong fluvial imprint, which is poorly defined or absent in similar-sized basins of a pronounced glacial or landslide legacy (Figure 4). There, long profiles show marked convexity, caused by hanging valley mouths, glacially scoured bedrock knobs and steps, and deep-seated landsliding.

[15] Supposing that gorge cutting indeed was limited to the Holocene exclusively requires average bedrock incision rates of $E > 20$ mm yr^{-1} to explain the present height of most of the gorge walls (Table 2). These tentative rates are extremely high for the European Alps, and rival those in tectonically more active mountain belts [*Burbank et al.*, 1996], although pulses of elevated bedrock incision are also documented in regions of low uplift [*Reusser et al.*, 2004]. *De Graaff* [1996] reported values of $E < 5$ mm yr^{-1}, measured on stream boulders and bedrock surfaces over five years in nearby Austrian basins underlain by flysch and crystalline rocks. *Jäckli* [1957] noted rates of up to 8 mm yr^{-1} on the basis of historic abrasion of torrent control structures mantled by calc-schists similar to those in the Bündner schist units. Although high in their own right, they are most likely not representative of the mean postglacial erosion rates of <2 mm yr^{-1} [*Hinderer*, 2001]. Also, none of the historically observed high rates match those required for cutting the gorges during the Holocene exclusively.

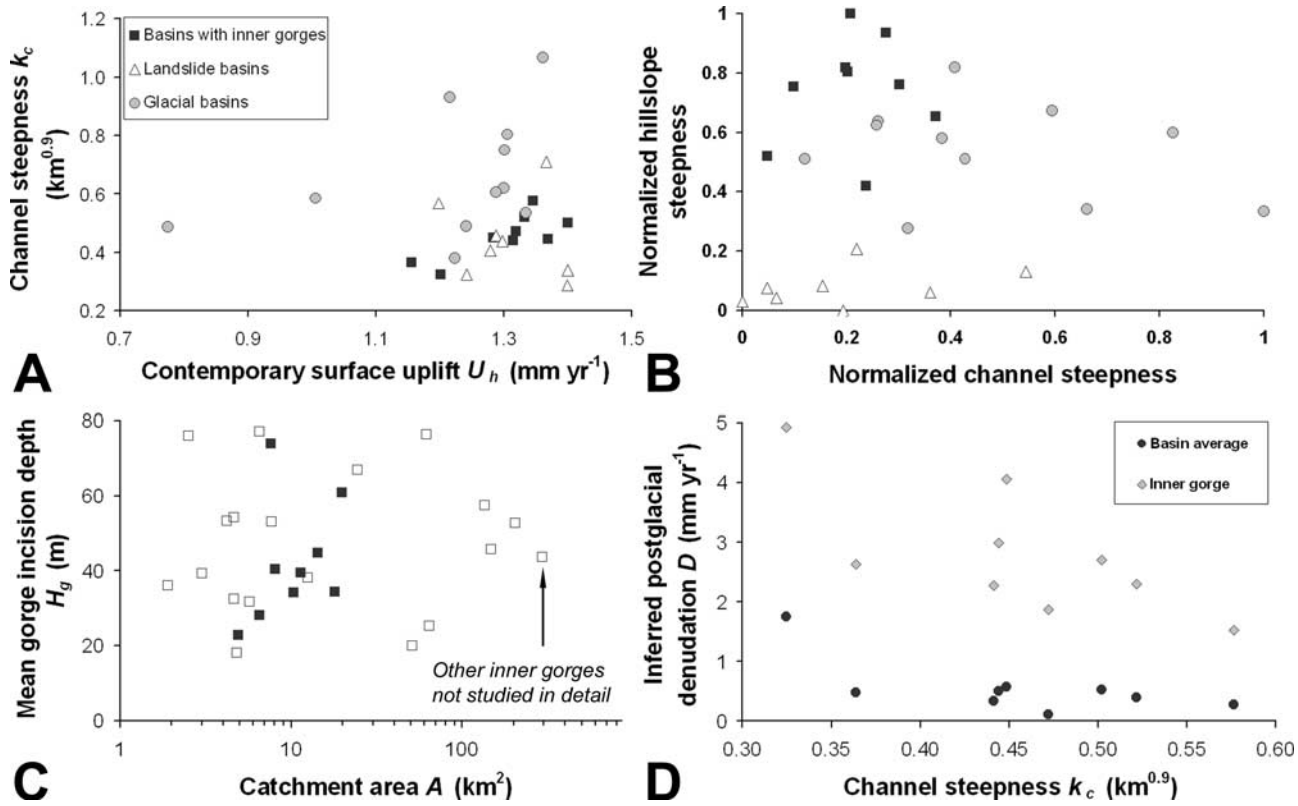

Figure 7. Scatterplots indicating landscape disequilibrium and transient geomorphic hillslope-channel coupling. (a) Independence of mean channel steepness k_c of historic surface uplift rate U_h derived from precision surveys. (b) Invariance of hillslope steepness with channel steepness, both normalized by range of values (symbols as in Figure 7a). (c) Mean depth of gorge incision versus upstream catchment area in studied (solid squares) and additional basins not further investigated (open squares). (d) Negative trend ($R^2 < 0.5$) of inferred postglacial denudation with k_c for basins with inner gorges.

5.2. Postglacial Sediment Yields

[16] The volume of material removed from the inner gorges necessitates estimated specific basin yields $Q_{s} = 2.8–4.2 \times 10^3$ m^3 km^{-2} yr^{-1} during the Holocene on average (Table 2 and Figure 7d). These yields are of the same order of magnitude as mean erosion rates back calculated from the volumes of perialpine lake sediment storage, i.e., 1–2 mm yr^{-1} [*Hinderer*, 2001], especially when considering that historic Q_{s} from basins underlain by Bündner schist and flysch is amongst the highest in the Alps. Where steep torrents undercut large schist sackung-type landslides, Q_{s} may attain up to >3 $\times$ 10^4 m^3 km^{-2} yr^{-1}, dominantly transported during large debris flows [*Huder*, 1976; *Ziegler*, 1982]. *Jäckli* [1957] estimated that individual sackungen delivered to the drainage network an annual average lateral input between 0.6 and 15 m^2 of sediment per unit length of basal channel. For comparison, denuding a cross section of 300-m-high inner gorge walls inclined at 45° by parallel slope retreat, at a rate of 20 mm yr^{-1}, would produce 6 m^2 per unit channel length. Large postglacial alluvial and debris flow fans sourced from small tributary basins in Bündner schists prograde onto the broad Vorderrhein valley floor, and provide a means to interpolate sediment yields over the Holocene. We estimated the volumes of these fans spanning most of the present valley floor width, and covering trunk-river alluvium that lies discordantly over hummocky debris of the 9-ka-old Flims rockslide [*Von Poschinger*, 2005] (Figure 1b). The inferred rates range from 0.04 to 2.5 $\times$ 10^4 m^3 km^{-2} yr^{-1}, and most likely apply to bed load only. Considering a more conservative immediate post-LGM onset of fan formation still requires average basin denudation rates of $D = 5–13$ mm yr^{-1}.

[17] The question is whether these high rates of postglacial sediment yields have been facilitated mainly by bedrock erosion or by removal of valley fills. The latter possibility is indicated by pockets of tentative glacial and fluvioglacial deposits preserved along parts of some gorge walls and several debris-filled and deeply incised slot gorges [*Cadisch*, 1926; *Jäckli*, 1957]. In the Landquart valley, we found that the 1.5-km^2 postglacial alluvial fan of the Ariesch torrent (immediately south of basin 19, Figure 1a) is perched on top of its tributary junction cut in bedrock; what appears to be fanhead trenching is actually incision of at least 20 m into Bündner schist bedrock. The presence of such sediment fills in gorges >100 m deep constrains any preceding bedrock incision to the early Holocene, and it is thus likely that a number of gorges existed prior to this period. Unfortunately, neither contemporary sediment yields nor the present degree of alluvial cover in some of the gorge floors can be taken as an indication of any long-term transport conditions because of extensive torrent control in many small basins in the study area. This includes affores-

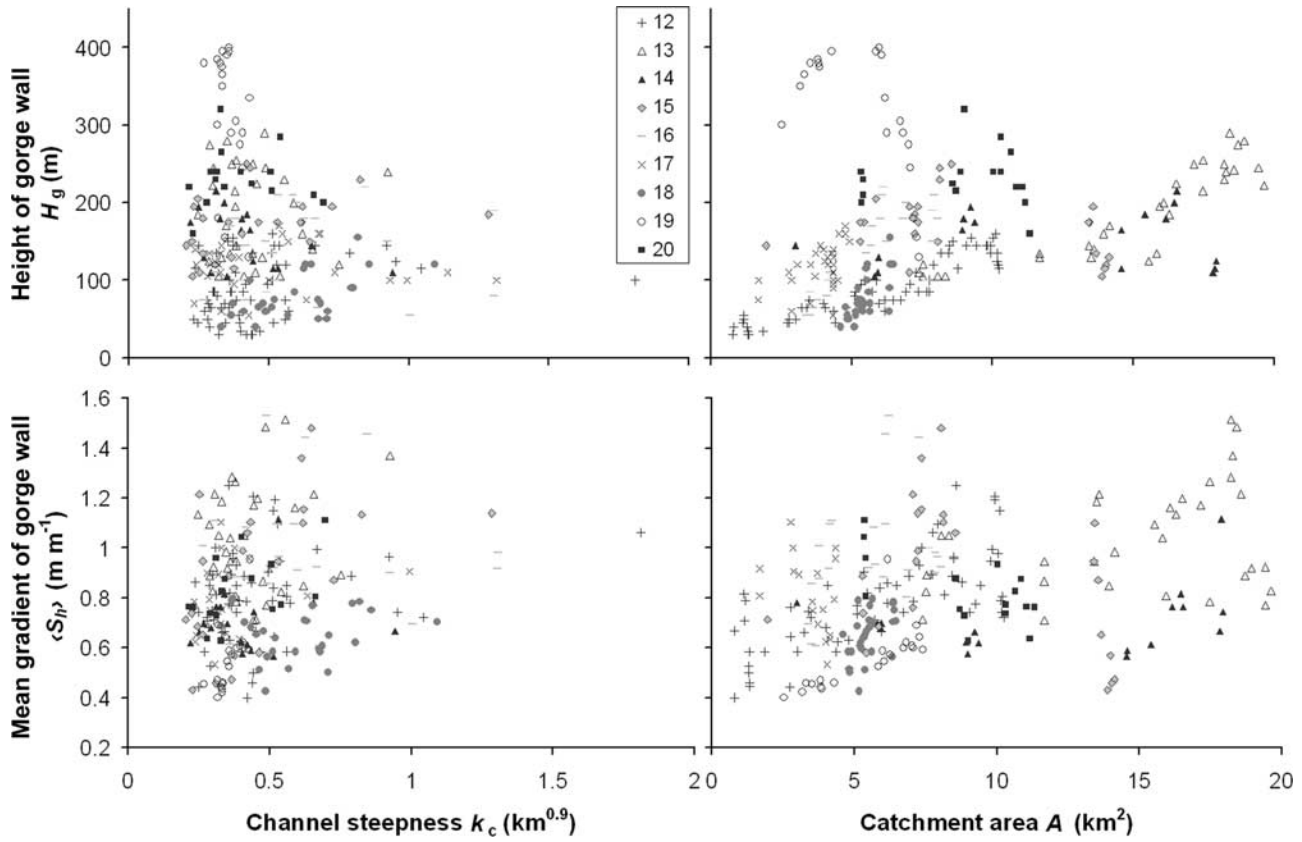

Figure 8. Morphometric properties of inner gorges (numbers refer to Table 1). Note poor relationships between height of gorge walls H_g, their mean gradients $\langle S_h \rangle$, and k_c, despite well-defined channel concavity (Figure 4).

tation measures, which may partly explain the forest stands on some of the gorge walls.

5.3. Bedrock Landsliding

[18] Rapid postglacial fluvial bedrock incision with active headward knickpoint migration of the rates sketched above would strongly promote, if not require, the formation of threshold hillslopes. DEM-derived slope area data yield values of $\theta_h \sim 0$ that formally resemble the theoretically predicted $\langle S_h \rangle - A$ plots for threshold hillslopes (Figure 9) [*Tucker and Bras*, 1998]. Also, the correlation between k_c and mean hillslope gradients $\langle S_h \rangle$ along the inner gorges is weak (Figure 8). A comparable situation was noted, for example, by *Safran et al.* [2005] in the Bolivian Andes, who argued for a threshold state in hillslope development, which, because of frequent landsliding, was insensitive to varying fluvial incision rates. The amount of *average* vertical incision is independent of catchment area A (Figure 7c), although the inferred rates of postglacial denudation decrease with increasing k_c. If k_c is indeed acceptable as a proxy for fluvial erosion potential, this seemingly counterintuitive instance can be explained by the transient state of steeper channels that have not yet managed to achieve their full incision potential, all other influences such as erodibility or sediment flux being constant.

[19] Another important observation is that these tentative threshold conditions are largely limited to the lower 25% of local hillslope relief. In terms of geomorphic hillslope-channel coupling, the inner gorge walls thus essentially form most of the active hillslopes. Mass movement processes such as shallow landsliding, debris flow, or solifluction on the upper, more gently inclined, and larger portions of the hillslopes are largely decoupled from the channels, and may have undergone climatically driven activity phases during the Holocene [*Dapples et al.*, 2003] without any fluvial forcing. Only where steep ravines deliver sediment from the hillslopes directly into the channel, or where large (>10^6 m^3) and slope-clearing failures have in places obliterated inner gorge walls ("Ri" in Figure 10), is the geomorphic coupling of hillslopes and channels more pronounced. We point out that this spatially limited development of threshold hillslopes is not evident from slope histograms (Figure 5). Large postglacial, catastrophic bedrock landslides that have been emplaced into existing bedrock gorges provide further age constraints. For example, the removal of excessive landslide debris of up to 400 m thickness that blocked the Vorderrhein and several major tributaries near Flims around 9 ka (Figure 1b) has since impeded bedrock gorge cutting over large upstream reaches [*Von Poschinger*, 2005; *Korup*, 2006]. The neighboring giant (10^9 m^3) Tamins rockslide–rock avalanche, which is believed to have occurred shortly after the Flims event, has truncated small bedrock gorges, which therefore must predate catastrophic detachment of the rock mass (Figure 2b).

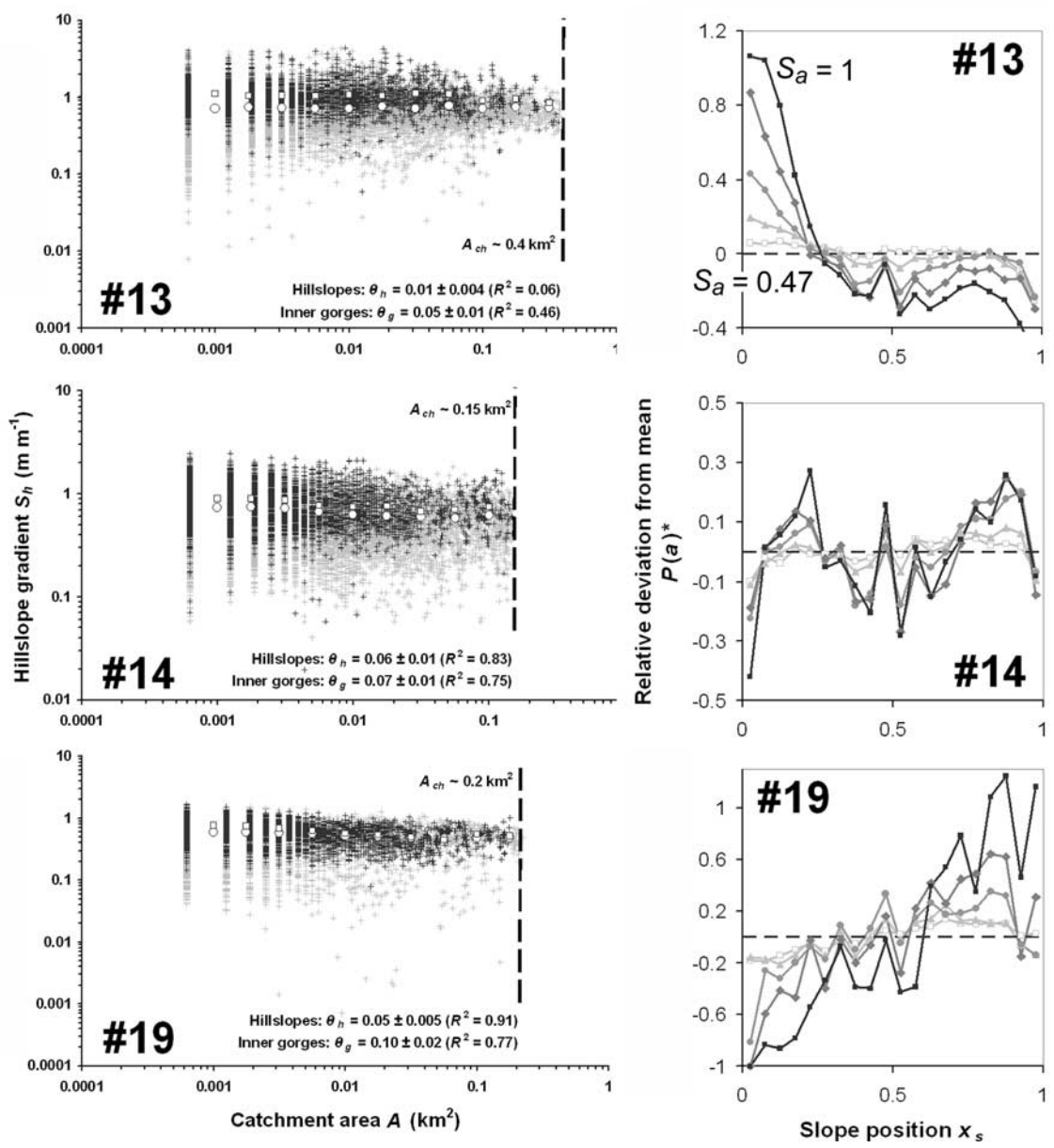

Figure 9. Slope-area and slope-distribution plots of upper hillslopes (gray pluses; bin-averaged, open circles) and gorge walls (black pluses; bin-averaged, open squares) of selected basins. Slope distribution plots show relative deviation from the mean of probability density $P(S_h \geq S_a)$ of slope position x_s (0, channel; 1, divide) within bins of width $\Delta x_s = 0.05$, for various values of S_a (see text for explanation). Note variable distribution of S_h with x_s despite well-defined inner gorges.

These observations support the notion of a pre-Holocene onset of gorge cutting.

[20] A number of presumably Holocene slow-moving landslides commonly involving 10^8–10^9 m^3 on dip slopes also maintain hillslope adjustment to fluvial incision. These sackung failures effectively counteract fluvial incision by horizontal rock mass advection documented by historically measured rates of differential slope deformation of 10^0–10^3 mm yr^{-1} [*Ziegler*, 1982], clearly outpacing regional rates of surface uplift. This close geomorphic coupling has created asymmetric valley cross sections, and prevented the formation of continuous inner gorges. From a regional kinematic analysis we find that slope adjustment of inner gorge walls by landsliding is strongly controlled by the orientation of the schist bedding planes. Even hillslopes with low bedding-dip angles (i.e., 15–25°) may be prone to large slow-moving landslides [*Jäckli*, 1957]. Conversely, inner gorges appear to be preferentially cut normal to the strike of major bedding planes on counterdipping opposite valley walls (Figures 2c and 10). Geometrically, this requires that toppling combined with sliding are important processes for fluvial bedrock detachment, whereas small-scale wedge failures mobilize rock from the inner gorge walls (Figure 3b). This complements the findings of *Miller* [1999], who observed a consistent alignment of channel slope with the dip of carbonate strata in bedrock rivers of south-central Indiana.

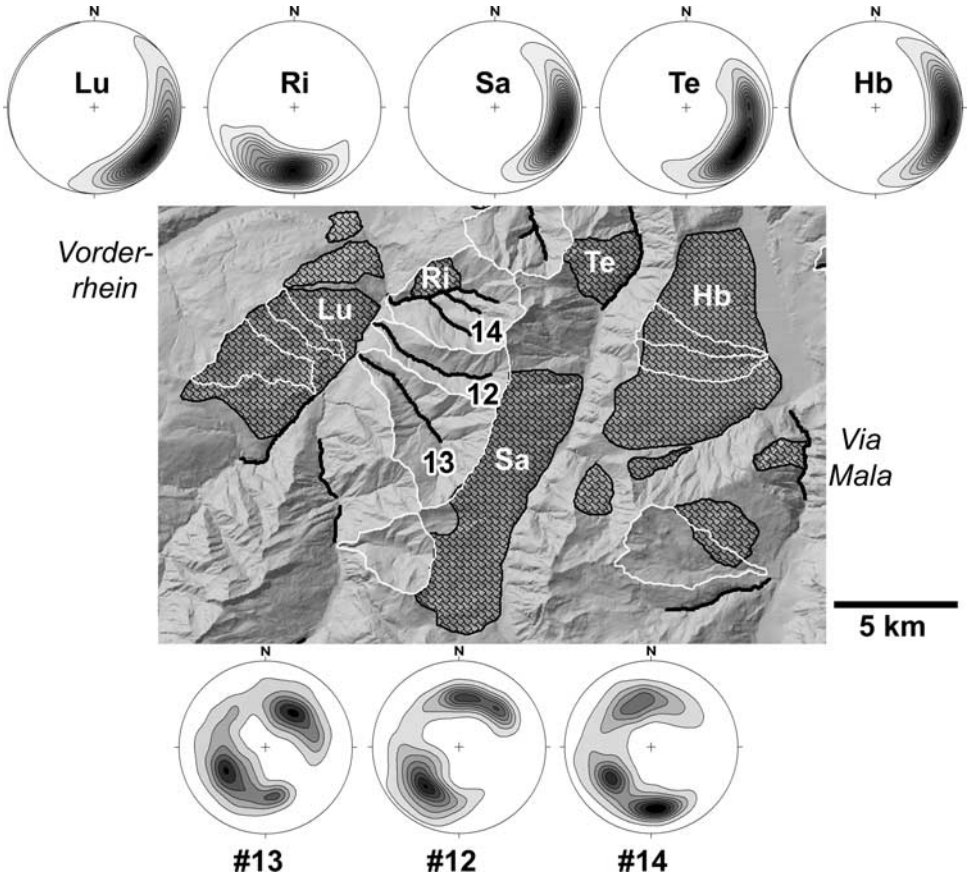

Figure 10. Lower hemisphere plots with equal area density contours at 1% spacing of slope azimuth and gradient. Overall strike/dip of major bedding planes in Bündner schist in this area is NE–SW/20° ± 5°. Note susceptibility of such low-angle dip slopes to large-scale sackung-type landsliding (patterned areas: Lu, Lumnez; Ri, Riein; Sa, Safien; Te, Tenna; Hb, Heinzenberg), as opposed to preferential cutting of inner gorges (black lines) into juxtaposed counterdip slopes.

5.4. Postglacial Versus Pre-Holocene Age of Inner Gorges

[21] In summary, we find that field observations and geomorphometry support two plausible, yet contrasting scenarios, which postulate either a postglacial or a pre-Holocene onset of gorge cutting. The first scenario explains the origin of the inner gorges by headward knickpoint migration in response to changes in base level fall rate. Bedrock incision theory predicts a kinematic wave response to changes in uplift under detachment-limited conditions. As the base level signal propagates upstream, migrating knickpoints separate downstream reaches adjusted to base level fall from upstream reaches subject to further slope replacement [*Whipple and Tucker*, 2002], while adjacent hillslopes are oversteepened by elevated erosion rates [e.g., *Ahnert*, 1988]. Because the Alpenrhein catchment was almost fully glaciated during the LGM, this scenario of relief rejuvenation requires postglacial fluvial bedrock incision into a glacially shaped geomorphic surface [*Schlunegger and Hinderer*, 2003]. Gorge incision would thus have been caused climatically, with decaying glaciers in overdeepened trunk valleys driving local base level falls that were communicated upstream from tributary junctions, and possibly enhanced by meltwater discharge through proglacial gorges from degrading cirque glaciers [e.g., *McEwen et al.*, 2002; *Meigs et al.*, 2006].

[22] The second scenario argues for a pre-Holocene onset of gorge cutting, as most of the basins with inner gorges are tributaries of valleys that have been repeatedly glacially scoured during the Pleistocene. The occurrence of hanging tributaries and waterfalls along some of the gorges suggests a subglacial phase in their evolution, although *Stock et al.* [2005] pointed out the possibility of fluvial hanging valleys. Nevertheless there may have been subglacial mechanisms conducive to gorge incision [*Shreve*, 1972]. Although tunnel valleys are known to have developed under continental ice sheets [e.g., *Hooke and Jennings*, 2006], little is known about the preservation of larger subglacial bedrock channels in alpine terrain, let alone representative rates of subglacial or postglacial bedrock incision [*Brocard et al.*, 2003]. *Eyles et al.* [1990] found that several of the glacial overdeepened lake basins in the interior plateau of British Columbia featured massive sediment fills above a v-shaped bedrock topography with depths of ~650 m below sea level, and followed that Wisconsinan glaciers had accentuated bedrock relief along preglacial and structurally controlled drainage lines. Conversely, several studies argued for a protective effect of large-scale glaciations [*Garwood*, 1910], on the basis of the limited occurrence of glacial

deposits in some inner gorges. With few absolute age constraints, this lends limited support to the notion that incision of at least a number of inner gorges had begun prior to the Holocene [*Cadisch*, 1926; *Tricart*, 1960; *De Graaff*, 1996]. This requires the preservation of gorge relief beneath a protective sediment fill. Such fill could have been contributed in parts by ice-marginal deposits following tributary blocking by trunk glaciers, and subsequent burial by proglacial deposits from growing tributary cirque glaciers [*De Graaff*, 1996].

6. Constraints From Slope Stability Modeling

6.1. Model Rationale

[23] In the following, we further explore the possibility of rapid postglacial cutting of the inner gorges in the study area. We surmise that the required high rates of fluvial bedrock incision should prompt the formation of threshold hillslopes (Figure 8). Here we used a simplistic slope stability model as a test of whether the inner gorge walls in the study area are indeed in a state conducive to frequent landsliding in concert with rapid gorge cutting. The literature is almost devoid of mechanistic approaches to explicitly test the concept of threshold hillslopes [*Montgomery*, 2001]. *Schmidt and Montgomery* [1995] argued that, at the landscape scale, hillslope relief is limited by either rock mass strength or fluvial incision. They used the Culmann wedge failure criterion for dry soil cliffs to derive the maximum stable hillslope height H_c,

$$H_c = \frac{4c \sin\beta \cos\phi}{\gamma_r[1 - \cos(\beta - \phi)]}, \tag{5}$$

where c is cohesion, β is mean hillslope angle, ϕ is the angle of internal friction, and γ_r is the mean unit weight of the slope material.

[24] On the basis of our observations of failure processes on inner gorge walls, we chose a limit-equilibrium approach more applicable to an oversteepened rock slope. This model assumes planar sliding of a trapezoidal block below a vertical tension crack (Figure 3c). The ratio of hillslope strength to effective shear stress is expressed as

$$F_S = \frac{c' A_s + (w\cos\psi - u - v\sin\psi)\tan\phi}{(w\sin\psi + v\cos\psi)}, \tag{6}$$

where F_S is the factor of safety, c' is the cohesive strength of the failure plane, A_s is the area of the failure plane, ψ is the angle of the failure plane, w is the weight of the rock block above the failure plane, u is the uplifting water force along the failure plane, and v is the driving water force along the tension crack [e.g., *Wyllie and Mah*, 2004]. Equation (6) can be written in dimensionless groups as

$$F_S = \frac{\dfrac{2c'}{\gamma_r H_g} p + \left(\dfrac{q}{\tan\psi} - r(p+s)\right)\tan\phi}{q + \dfrac{rs}{\tan\psi}}, \tag{7}$$

with

$$p = \frac{\dfrac{1}{\tan\beta} + x}{\cos\psi} \tag{8}$$

$$r = \frac{\gamma_w}{\gamma_r}\frac{z_w}{z}\frac{z}{H_g} \tag{9}$$

$$s = \frac{z_w}{z}\frac{z}{H_g}\sin\psi \tag{10}$$

$$x = \frac{b}{H_g} \tag{11}$$

$$y = 1 - \frac{\tan\psi}{\tan\beta} \tag{12}$$

$$q = \left(\frac{y}{\tan\beta} + 2xy + x^2(\tan\alpha - \tan\psi)\right)\sin\psi, \tag{13}$$

where γ_w is the unit weight of water, z is the depth of the vertical tension crack, z_w is the depth of water in the tension crack, H_g is the height of the inner gorge wall, b is the horizontal distance of the crack from the crest of the gorge wall, and α is the slope angle of the upper hillslope above the gorge (Figure 3c). For cohesionless slopes ($c' = 0$), stability thus depends only on slope geometry, but not on slope size. This makes it applicable to small block slides as well as large slope-clearing failures. For all other cases, we expect F_S to decrease nonlinearly with slope height H_g, for a given slope geometry.

[25] Equations (9) and (10) allow inclusion of transient loading due to cleft water pressures along the tension crack and the potential sliding plane. Another advantage of the trapezoidal model is that it states a general form of a series of special cases for which the critical hillslope height H_c at limit equilibrium (i.e., $F_S = 1$) may be derived. For example, we find that, for shallow failures on a fully drained slope ($z,\ b \to 0$),

$$\lim_{z,b\to 0} H_c = \frac{2c'}{\gamma_r \sin\psi\cos\psi\left(1 - \dfrac{\tan\psi}{\tan\beta}\right)\left(1 - \dfrac{\tan\phi}{\tan\psi}\right)}. \tag{14}$$

This is equal to the expression for planar rock slides on a dip slope where $\psi < \beta$ [*Selby*, 1992],

$$H_c = \frac{2c'\sin\beta}{\gamma_r \sin(\beta - \psi)(\sin\psi - \cos\psi\tan\phi)}. \tag{15}$$

Simplifying further for the limit case of a fully drained vertical gorge wall with daylighting potential failure planes [e.g., *Cruden*, 1976], where $\beta = 90°$, and $\alpha = \psi$, we obtain

$$H_c = \frac{2c'}{\gamma_r \cos\psi(\sin\psi - \cos\psi\tan\phi)} \tag{16}$$

as a simple model of parallel slope retreat. Values of ψ are usually difficult to predict. However, the angle of the critical failure plane ψ_c in a dry rock slope can be approximated by computing for which value of ψ limit equilibrium is most

readily reached, i.e., setting $\partial F_S/\partial\psi = 0$ in equation (7) [*Wyllie and Mah*, 2004], thus obtaining

$$\psi_c = \frac{1}{2}(\beta + \phi). \tag{17}$$

We note that substitution of equation (17) into equation (15) produces results very similar to those of the Culmann method (equation (5)) for low values of c'.

[26] Planar rock slope failures described by equation (6) require tight geometric preconditions [*Wyllie and Mah*, 2004]. These are not met everywhere along the gorge walls, particularly where rock parcels detach by other mechanisms such as fall, topple, rotational sliding, or along two intersecting sliding planes. Factors of safety for more common wedge failures (Figure 3b) are usually higher than those predicted by equation (6) by a wedge shape factor K_w, assuming that ϕ and ψ are equal for both failure planes. *Wyllie and Mah* [2004] suggest that $1 < K_w < 5$ for most cases. They argue that, for $F_{Sw} > 2$, dry cohesionless rock slopes are generally stable over a wide range of dynamic loading conditions. Therefore equation (6) is a practical and conservative first-order approximation of a variety of failure scenarios.

6.2. Mechanistic-Probabilistic Approach to Threshold Hillslopes

[27] The few published values of the apparent cohesive strength c' of Bündner schist range between 6 and 120 kPa for fragmented samples, for a unit weight of 19–22 kN m^{-3}, and an angle of internal friction of 23–30° [*Huder*, 1976; *Ziegler*, 1982]. Following the method of *Marinos and Hoek* [2001], our field estimates of the Geological Strength Index (GSI) are between 15 and 40, suggesting a range of c' = 300–800 kPa, and ϕ = 16–33°. Because of these substantial ranges, and our interest in potential threshold conditions at the regional scale, we performed a Monte Carlo simulation on equation (6). Together with the rock mass properties, we varied H_g such that we assigned a random value between 0 and 300 m (Table 3). This covers most of the relief of inner gorges, while also allowing for failures of portions of the gorge walls where failure planes dip out of the slope. The Monte Carlo method is a probabilistic first-order test of threshold conditions along the inner gorge walls. Statistically speaking, the majority, i.e., >50%, of gorge walls should be inclined at an angle conducive or close to failure [*Burbank et al.*, 1996]. We used a coefficient of reliability r_c that states the percentage of simulations where $F_S < 1$; the probability of failure is given by $1-r_c$. Thus $r_c = 1$ implies that all gorge walls are theoretically stable under the conditions chosen. It follows that a possible criterion for threshold hillslopes is $r_c = 0.5$, which implies that half of the gorge walls that the model readily applies to are potentially unstable. In other words, we suggest a median $F_S = 1$ as a quantitative indicator of the presence of threshold hillslopes, while fully allowing for any spatial variability of their occurrence. We ran the model for four slope conditions, i.e., fully drained (fd); fully saturated (fs); fully drained with undercut toe ($\alpha = 0$, fdc); and fully saturated with undercut toe ($\alpha = 0$, fsc; Figure 11a). We determined the coefficient of reliability r_c as a function of c' at intervals $\Delta c' = 10$ kPa. For each interval, we ran 5,000 simulations of equation (6), varying all parameters within field- and DEM-derived distributions (Table 3).

[28] Simulation results show that dry slopes attain $r_c = 1$ at $c' = 175$ kPa, while fully saturated slopes do so at $c' = 275$ kPa (gray vertical lines in Figure 11). We term these two values the strength limits. Any decrease in c' below these limits because of weathering will result in an increase in the probability of failure due to loss of hillslope strength, so that the maximum stable gorge wall height is mainly strength limited. Increases in c', conversely, will not affect this probabilistic stability, although it will raise F_S on average and hence "excess" stability. In other words, without any changes to rock mass properties, instability above these strength limits is only possible, if the slope geometry is altered by fluvial incision. Hence the maximum gorge wall height is mainly incision limited. The simulation suggests that toe undercutting does little to increase the probability of failure near the strength limits, but substantially contributes to destabilizing slopes at lower values of c' (Figure 11a). The worst-case scenario is given by the curve that is a fully saturated slope with toe undercut (fsc). Assuming a probabilistic threshold hillslope state ($r_c = 0.5$), we obtain apparent cohesive strengths of about 20 kPa and 120 kPa for fully drained, and fully saturated slopes, respectively (Figure 11a). We term these values the threshold hillslope strengths. Because median $F_S \propto c'$ (equation (6)), any alternative criterion for the presence of threshold hillslopes based on the median F_S must also be a function of cohesive strength.

[29] We used the strength limits derived from Figure 11a to compute the critical height a given gorge wall is able to sustain before planar failure (equations (15) and (16)). We also plotted curves for potential circular failure planes, which we derived from slope stability charts [*Wyllie and Mah*, 2004]. We test the applicability of these model curves by comparing them to the heights and mean gradients of gorge walls derived from the DEM (Figure 11b). The plot suggests that most slopes can be considered stable when using a simple dip slope model under fully drained conditions (Dd, equation (15)). With regard to circular failure planes (Rd), about 10% of the gorge walls plot above the theoretically possible height limit, indicating potential failure by slumping. We infer that the model simulation either underestimates the rock mass properties, or that conditions for rotational failure are not fully met at these sites, while other failure models might be more adequate. The probability of failure roughly doubles for fully saturated conditions (Rs, Figure 11b). Back calculations for a rotational landslide that affected 2.5 km^2 of the northern part of basin 14 ("Ri", Figure 10) indeed suggests that the valley flank would have been stable under fully drained conditions, whereas fully saturated conditions could have triggered failure. The landslide toe has been further trimmed to slope angles that now appear more stable with respect to rotational failure (arrowed triangles in Figure 11b). The largest theoretical instability is predicted by the model of parallel-retreat slopes undercut by a vertical cliff (cDd, equation (16)), though in this case the H_c solely applies to the cliff section. Because we did not find vertical portions of gorge walls in excess of about 20 m in the field, we regard this model to be rather conservative.

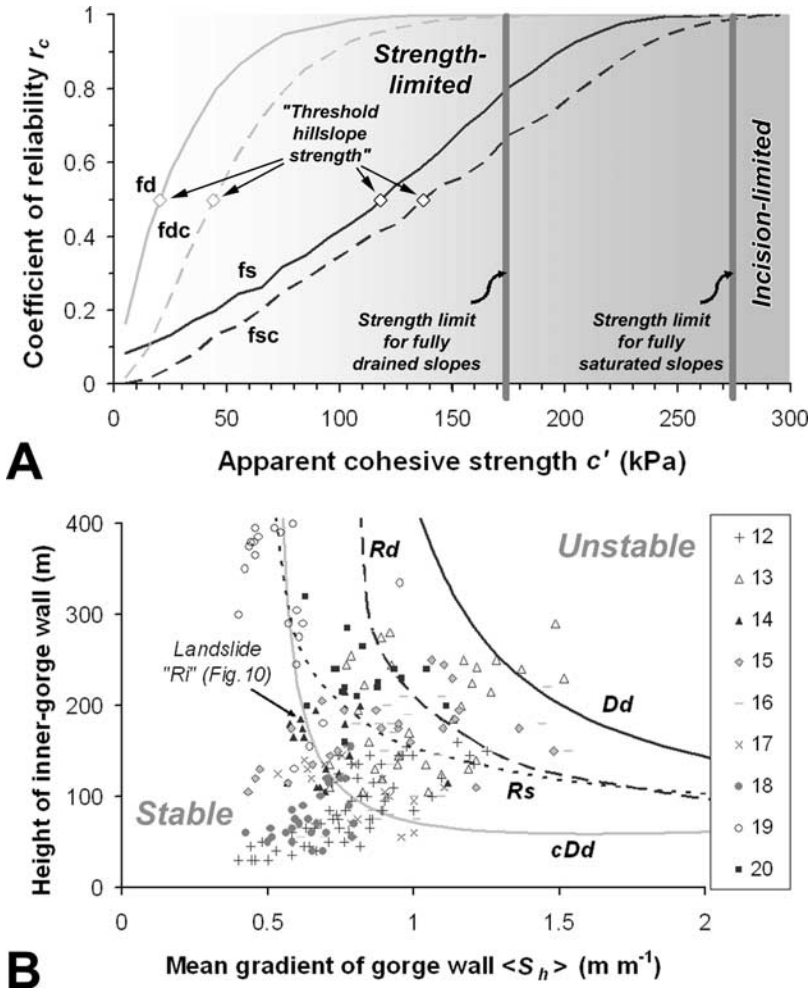

Figure 11. Model rock slope stability against planar failure of inner gorge walls, obtained from Monte Carlo simulation ($n = 5000$ for each $\Delta c' = 10$ kPa; for parameters, see Table 3). (a) Coefficient of reliability r_c as a function of c' for fully drained slope (fd); fully drained slope, undercut toe ($\alpha = 0$, fdc); fully saturated slope (fs); and fully saturated slope, undercut toe ($\alpha = 0$, fsc); $r_c = 1$ defines strength limits (gray vertical lines for cases without undercuts only) of $c' \sim 175$ kPa and $c' \sim 275$ kPa for dry and saturated slopes, respectively. Threshold hillslope strength for each scenario is derived at $r_c = 0.5$. (b) Relationship between height and mean gradient of inner gorge walls, plotted together with curves for critical hillslope heights, using strength limits derived from (Figure 11a) for fully drained dip slope model (Dd, equation (15)), fully drained slope with circular failure plane (Rd), fully saturated slope with circular failure plane (Rs), and vertical cliff in fully drained dip slope (cDd, equation (16)). See text for explanation.

6.3. Strength and Incision Limits

[30] The Monte Carlo approach provides conservative probabilistic limits of planar rock slope stability set by cohesive strength (Figure 11). Frequent wetting and drying, freeze-thaw cycles, and rapid weathering of soft Bündner schist and flysch rocks play important roles in reducing slope stability. Conversely, fluvial incision leads to release of tectonic strain energy [*Huder*, 1976], causing slope dilatation and further destabilization. We therefore use equation (15) as an example to anticipate the relative importance of strength limitation over incision limitation through time, as weathering reduces c', while fluvial downcutting into bedrock increases H_g. Both processes contribute to reducing F_S, and gradually attaining the critical slope height H_c. Equations (15) and (16) imply that with slope geometry and internal friction angle remaining constant, H_c is a linear function of c'. *Howard* [1998] modeled gradual loss of cohesion through weathering as

$$c'(t) = c_0 e^{-\lambda(t-t_0)}, \tag{18}$$

where c_0 is the initial cohesion at initial time t_0, and λ is the mean weathering rate, and which in this case does not alter ϕ. From equations (15) and (16) we obtain for $t_0 = 0$:

$$H_c(t) = \frac{2c_0 e^{-\lambda t}}{\gamma_r \Lambda}, \tag{19}$$

and

$$H_g(t) = H_0 + Et, \tag{20}$$

Table 3. Field- and DEM-Derived Parameter Ranges Used for Monte Carlo Simulation of Planar Rock-Slope Stability Along Inner Gorges

Parameter	Distribution	Mean	σ	Other	Units	Source
α	normal	30	2	-	deg	25-m DEM
b	random	1	0.3	-	m	field observations of typical slope-failure depths
β	normal	39	2	-	deg	25-m DEM
β_0	random	80	1	$\alpha = 0$	deg	field observations on typical overhang angles at undercut gorge walls
γ_r	uniform	-	-	19	kN m^{-3}	*Huder* [1976], *Ziegler* [1982]
γ_w	uniform	-	-	10	kN m^{-3}	unit weight of water
H_g	random	-	-	$\eta \in [0,300]$	m	25-m DEM
H_u	random	-	-	$\eta \in [0,10]$	m	field observations on typical undercuts
ϕ	normal	26	3	-	deg	average of several published values [*Huder*, 1976; *Ziegler*, 1982], including measurements at residual strength
ψ_c	-	-	-	$(\beta + \phi)/2$	deg	*Wyllie and Mah* [2004]
z_w/z	uniform	-	-	0	-	fully drained slope
z_w/z	uniform	-	-	1	-	fully saturated slope

for weathering-induced, and incision-induced rock slope failure, respectively, where H_0 and H_c' are gorge relief, and critical (strength-limited) gorge relief, at time t_0, respectively, and Λ is a dimensionless coefficient describing the slope geometry and its internal friction. We can thus estimate the time theoretically required for a gorge wall to fail by attaining the strength limit (Figure 12).

[31] This simple model neglects any climatic variability that may affect λ over the timescales considered. Also, assuming E to be constant throughout excludes effects of knickpoint migration, and requires that incising rivers remain below capacity as to maintain detachment-limited conditions despite increasing rates of hillslope sediment yields, as gorge relief and hillslope lengths grow. Moreover, maintained exposure of fresh bedrock by landsliding in response to high rates of fluvial incision may effectively limit weathering. Nevertheless, the model is, to our best knowledge, the first approach to depict within a framework of field data the relationship between rock strength, fluvial incision rate, weathering rate, and inner gorge relief along a bedrock river flanked by oversteepened rock slopes.

[32] We stress that the limit-equilibrium model used is a simplistic and first-order approach to probabilistically testing the presence of threshold hillslopes at the regional scale, bearing several caveats. First, the anisotropic rock mass properties of Bündner schist and flysch violate the model assumption of uniform slope materials [*Margielewski*, 2006]. However, this is a common problem in many slope stability assessments, and not confined to this study. The Monte Carlo method and back calculation of c' is one way of overcoming and quantifying some of this uncertainty through a coefficient of reliability. We are under no illusion that this probabilistic approach goes much beyond a crude regional estimate, which is what we intended in the first place. It is *not* a surrogate of site-specific slope stability, especially as many other controls on rock mass strength, among others, vegetation, weathering (besides the ones sketched above), and neotectonics, are not included. It is, however, a consequential extension of earlier attempts to model thresholds and limits in hillslope response to fluvial incision [*Schmidt and Montgomery*, 1995; *Burbank et al.*, 1996; *Montgomery*, 2001]. Second, the kinematic requirements for the plane-strain model are not met everywhere along the inner gorge walls. In fact, large-scale sackung-type landslides that slowly reduce slope angles at the scale of whole valley flanks have developed on most dip slopes (Figures 4 and 10). *Ziegler* [1982] showed that several slopes subject to such deep-seated creep failure should be considered metastable, as back calculations have returned values of $1 < F_S < 1.5$. Nonetheless, Figure 11 covers basic scenarios for rotational landslides, and sets lower bounds for wedge failures; our findings on strength and incision limitation are strictly valid for these failure modes, and within the specified parameter spaces (Table 3). Third, we point out that our analysis did not touch upon other possible mechanisms of hillslope adjustment toward a threshold state, such as gullying or debris flow on weathered rock slope portions (Figure 2c).

6.4. Implications

[33] Despite these limitations, slope stability modeling provides two important insights, albeit for a set of special cases. First, it offers a mechanistic rationale to quantitatively define a threshold state in hillslope development expressed by a probabilistic coefficient of reliability (Figure 11a). Second, it provides estimates of strength and incision limits that are averaged over a range of possible conditions. These can be used to estimate the critical gorge wall height as a function of its mean gradient, thus making comparison of model with field data possible. The theoretically derived strength limits (Figure 11a) seem unduly high for fragmented Bündner schist and flysch rocks exposed in many gorge walls. Lower, and possibly more realistic, values of c' imply that parts of the inner gorge walls are intrinsically unstable as a result of inner gorge cutting (Figure 11b). Field observations support the notion that the Bündner schists and flysch rocks most inner gorges are cut into are strength limited, thus prone to a variety of threshold slope failure mechanisms. The morphologically most pronounced is that of slow hillslope-scale sliding along dip slopes.

[34] In summary, we infer that the constraints on the age of inner gorges set by fluvial bedrock incision, postglacial sediment yields, and bedrock landsliding are ambiguous. Morphometric characteristics of inner gorges indicating profile adjustment and threshold hillslope formation due to sudden base level adjustment, intuitively guiding as they may be, must be treated with care, as there is the possibility of an unquantifiable amount of inheritance preserved in

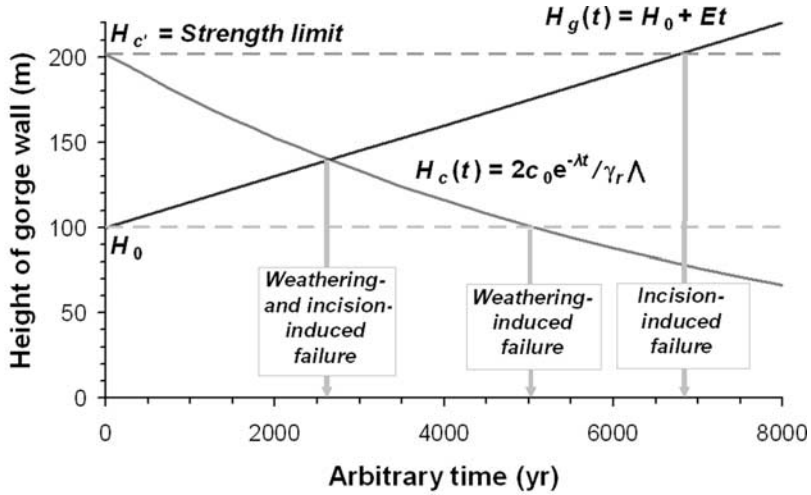

Figure 12. Schematic competition between weathering- and incision-driven rock slope failure with c_0 = 75 kPa, γ_r = 19 kN m^{-3}, ϕ = 26°, β = 44°, ψ = 35°, $\lambda = 1.38 \times 10^{-4}$ yr^{-1}, and E = 15 mm yr^{-1}. The initial strength-limited slope height, $H_c' \sim 200$ m (equation (19)), decreases exponentially with time because of weathering. For an arbitrary initial gorge wall height H_0 = 100 m and no fluvial incision (E = 0), weathering-induced failure occurs after 5 ka. Conversely, slope failure driven by (detachment-limited) incision in the absence of weathering (λ = 0) occurs after 6.8 ka, despite the high value of E. Combined weathering and fluvial incision will trigger slope failure after 2.7 ka.

these landforms. This inheritance of fluvial sculpted topography cannot be resolved sufficiently by morphometric analysis alone, although the seemingly contradictory field evidence can be reconciled by postulating that the present morphology of inner gorges in the study area bears imprints of both rejuvenation and inheritance. This leads us to speculate that a combination of the two scenarios is most likely, i.e., that many bedrock gorges in the study area have been cut in pre-Holocene times, and have been protected and rejuvenated during glacial and interglacial conditions, respectively. If this notion is realistic, one corollary is that the denudation by an extensive ice stream network was insufficient to obliterate the fluvial character of these gorges.

[35] We stress that, even without a specific date for the onset of gorge cutting, the associated erosion rates are high, outpacing the decadal-scale surface uplift rate by an order of magnitude. Judging from thermochronologic constraints [*Schlunegger and Willett*, 1999], the possibility that gorge incision responded to dramatic changes in postcollisional uplift is remote; however isostatic rebound or neotectonics may have played a significant role. On shorter timescales, e.g., repeated glacial-interglacial cycles, we propose a delayed hillslope response to fluvial bedrock incision modulated by climatic oscillations, i.e., repeated glacial-interglacial cycles.

[36] We refine the model of *Kelsey* [1988] by noting that weak and highly anisotropic rocks may also be subject to inner gorge formation, without invoking the need for solely parallel retreat of gorge walls. Moreover, the inner gorges we studied are contiguous, and not randomly dispersed, landforms, so that we can infer a systematic response to a forcing mechanism instead of a stage in normal hillslope development [*Densmore et al.*, 1997]. Finally, because large slope-clearing landslides mainly involve persistent deep-seated creep, it is possible that inner gorges could have never fully developed at the toes of sackungen instead of having been removed episodically by catastrophic failures.

[37] Future research on inner gorges in the eastern Swiss Alps will need to better confine the absolute ages of the LGM geomorphic surfaces, as well as many of the undated sedimentary fills in the gorges themselves. This should be complemented by physical rate measurements of channel incision and gorge wall retreat. Finally, regional inventories of major inner gorges in the European Alps and other mountain belts could help further refining their relationship to lithology, rates of uplift and erosion, Quaternary climate cycles, and large-scale hillslope stability.

7. Conclusions

[38] Three distinctive types of tributary basins variably dominated by either glacial, fluvial, or landslide morphologies indicate a postglacial landscape transience in the Alpenrhein catchment. Prominent inner bedrock gorges cut into highly erodible Cretaceous Bündner schist and lower Tertiary flysch units underlying many of the "fluvial-type" basins attest to geomorphic decoupling of hillslopes from bedrock channels. Inner gorge long and cross profiles show a high morphometric resemblance to detachment-limited bedrock rivers rapidly adjusting to base level fall through incision and headward knickpoint migration. The assumption of postglacial incision in response to decaying trunk glaciers fits well with very high postglacial sediment yields of up to 10^4 m^3 km^{-2} yr^{-1}, derived from soft calc-schists subjected to mainly strength-limited threshold landsliding in response to channel incision, limited to the lower 25% of local hillslope relief. This transient state, in which hillslopes lag behind channel adjustments, is a further characteristic of a postglacial landform and process disequilibrium. Moreover, historic sediment yield attains 10^4 m^3 km^{-2} yr^{-1}, thus locally outpacing short-term surface uplift

rate U_h obtained over a comparable (i.e., 10^1 year) timescale by an order of magnitude. Likewise, both hillslope and channel metrics are independent of the contemporary pattern of surface uplift. Any tectonic forcing on gorge incision is thus considered remote.

[39] For some bedrock gorges, a pre-Holocene onset of formation is plausible. Subglacial preservation, if not enlargement or formation, of the inner gorges, requires that glacial erosion either (1) is limited in its efficiency to fully remove landforms of fluvial erosion most likely because the gorges were filled with sediment or (2) locally contributes to enhancing selective linear erosion. The strong fluvial overprint in inner gorges shows that the concavity index θ_c, contrary to previous notions, does record transient adjustments in mountain rivers. We propose that lithology and Quaternary glacial-interglacial cycles are the primary controls on the formation of inner gorges in the Alpenrhein catchment. Clearly, long-term trends in landscape evolution in the eastern Swiss Alps cannot be readily extracted from the present-day relief without clearly resolving the effect of inheritance and rejuvenation. We therefore caution against the sole use of topographic data when inferring the rates of landscape response to tectonic or climatic forcing. Finally, there is the possibility that gorge incision could have been similarly inherited in other formerly glaciated mountain belts.

Notation

- A drainage basin area, L^2.
- A_{ch} contributing catchment area at channel head, L^2.
- A_g area of inner gorge, L^2.
- A_s area of sliding plane, L^2.
- α angle of upper slopes above inner gorge, deg.
- b horizontal distance of tension crack from top of inner gorge, L.
- β hillslope angle, deg.
- c cohesion, $ML^{-1}\ T^{-2}$.
- c' cohesive strength of failure plane, $ML^{-1}\ T^{-2}$.
- c_c' critical cohesive strength for planar failure, $ML^{-1}\ T^{-2}$.
- c_0 initial cohesive strength, $ML^{-1}\ T^{-2}$.
- D mean basin denudation rate, $L\ T^{-1}$.
- E bedrock channel incision rate, $L\ T^{-1}$.
- $\langle E \rangle$ mean basin elevation, L.
- η random number.
- ϕ angle of internal friction, deg.
- F_S factor of safety for plane failure model.
- F_{Sw} factor of safety for wedge failure model.
- γ_r unit weight of rock, $ML^{-2}\ T^{-2}$.
- γ_w unit weight of water, $ML^{-2}\ T^{-2}$.
- H total basin relief, L.
- H_u height of slope undercut, L.
- H_c maximum stable slope height for strength-limited rock slopes, L.
- H_c' initial strength limit to gorge relief, L.
- H_g height of inner gorge wall, L.
- H_0 inner gorge relief at model time $t = t_0$, L.
- K_w wedge factor.
- k_c steepness index of channel, $L^{2\theta_c}$.
- k_h steepness index of hillslopes, $L^{2\theta_h}$.
- λ mean weathering rate, T^{-1}.
- Λ coefficient of slope geometry and internal friction.
- L_g length of inner gorge, L.
- n sample number.
- $Q_{s'}$ specific sediment yield, $L^3\ L^{-2}\ T^{-1}$.
- ψ angle of failure plane, deg.
- ψ_c critical angle of failure plane, deg.
- r_c coefficient of reliability of F_S.
- $\langle S_c \rangle$ mean channel gradient.
- $\langle S_h \rangle$ mean hillslope gradient.
- θ_c concavity index of channel; reference value $\theta_c' = 0.45$.
- θ_g concavity index of inner gorge walls.
- θ_h concavity index of hillslopes; reference value $\theta_h' = 0.07$.
- t time, T.
- u uplifting water force along failure plane, $ML\ T^{-2}$.
- U_h contemporary rate of surface uplift, $L\ T^{-1}$.
- v driving water force along vertical tension crack, $ML\ T^{-2}$.
- V_e apparent volume eroded from inner gorge, L^3.
- w weight of rock block above an inclined sliding plane, $ML\ T^{-2}$.
- x_d distance to basal channel, L.
- x_s normalized hillslope position (0 = channel, 1 = divide).
- x_u distance to hillcrest, L.
- z depth of vertical tension crack, L.
- z_w height of water column in vertical tension crack, L.

[40] **Acknowledgments.** All topographic data including those in the figures were derived from DHM25 © 2005 swisstopo (DV033492). We thank John Clague, Jamie Shulmeister, and Fiona Tweed for initial hints and discussions. Alex Densmore and Harvey M. Kelsey provided helpful reviews.

References

Ahnert, F. (1988), Modelling landform change, in *Modelling Geomorphic Systems*, edited by M. G. Anderson, pp. 375–400, John Wiley, Chichester, U. K.

Baillie, I. C., and C. Norbu (2004), Climate and other factors in the development of river and interfluve profiles in Bhutan, Eastern Himalayas, *J. Asian Earth Sci.*, *22*, 539–553.

Bonnet, S., M. Besnard, and J. V. den Driessche (2001), Drainage network expansion of the Salagou drainage basin (S. France): An example of relief response to recent climate change?, *Terra Nova*, *13*, 214–219.

Bousquet, R., R. Oberhänsli, B. Goffe, L. Jolivet, and O. Vidal (1998), High-pressure–low-temperature metamorphism and deformation in the Bündnerschiefer of the Engadine window: Implications for the regional evolution of the eastern Central Alps, *J. Metamorph. Geol.*, *16*, 657–674.

Brardinoni, F., and M. A. Hassan (2006), Glacial erosion, evolution of river long profiles, and the organization of process domains in mountain drainage basins of coastal British Columbia, *J. Geophys. Res.*, *111*, F01013, doi:10.1029/2005JF000358.

Brocard, G. Y., P. A. van der Beek, D. L. Bourlès, L. L. Siame, and J. L. Mugnier (2003), Long-term fluvial incision rates and postglacial river relaxation time in the French western Alps from ^{10}Be dating of alluvial terraces with assessment of inheritance, soil development and wind ablation effects, *Earth Planet. Sci. Lett.*, *209*, 197–214.

Burbank, D. W., J. Leland, E. Fielding, R. S. Anderson, N. Brozovic, M. R. Reid, and C. Duncan (1996), Bedrock incision, rock uplift, and threshold hillslopes in the northwestern Himalaya, *Nature*, *379*, 505–510.

Cadisch, J. (1926), Zur Talgeschichte von Davos, *Jahresber. Naturforsch. Ges. Graubuendens*, *59*, 285–299.

Cruden, D. M. (1976), Major rockslides in the Rockies, *Can. Geotech. J.*, *13*, 8–20.

Dapples, F., D. Oswald, H. Raetzo, T. Lardelli, and P. Zwahlen (2003), New records of Holocene landslide activity in the western and eastern Swiss Alps: Implication of climate and vegetation changes, *Eclogae Geol. Helv.*, *96*, 1–9.

De Graaff, L. W. S. (1996), The fluvial factor in the evolution of alpine valleys and of ice-marginal topography in Vorarlberg (W-Austria) during the Upper Pleistocene and Holocene, *Z. Geomorphol.*, *104*, 129–159.

Densmore, A. L., and N. Hovius (2000), Topographic fingerprint of bedrock landslides, *Geology*, *28*, 371–374.

Densmore, A. L., R. S. Anderson, B. G. McAdoo, and M. A. Ellis (1997), Hillslope evolution by bedrock landslides, *Science*, *275*, 369–372.

Eyles, N., H. T. Mullins, and A. C. Hine (1990), Thick and fast: Sedimentation in a Pleistocene fiord lake of British Columbia, *Geology*, *18*, 1153–1157.

Garwood, E. J. (1910), Features of Alpine scenery due to glacial protection, *Geogr. J.*, *3*, 310–336.

Hinderer, M. (2001), Late Quaternary denudation of the Alps, valley and lake fillings and modern river loads, *Geodin. Acta*, *14*, 231–263.

Hooke, R. L., and C. E. Jennings (2006), On the formation of the tunnel valleys of the southern Laurentide ice sheet, *Quat. Sci. Rev.*, *25*, 1364–1372.

Howard, A. D. (1998), Long profile development of bedrock channels: Interaction of weathering, mass wasting, bed erosion, and sediment transport, in *Rivers Over Rocks: Fluvial Processes in Bedrock Channels*, *Geophys. Monogr. Ser.*, vol. 107, edited by K. J. Tinkler and E. E. Wohl, pp. 297–319, AGU, Washington, D. C.

Huder, J. (1976), Creep in Bündner schist, in *Contributions to Soil Mechanics*, edited by N. Janbu, F. Jorstad, and B. Kjaernsli, pp. 125–153, Norw. Geotech. Inst., Oslo.

Jäckli, H. (1957), Gegenwartsgeologie des bündnerischen Rheingebietes, *Beitr. Geol. Schweiz Geotech. Ser.*, *36*, 136 pp.

Kahle, H. G., et al. (1997), Recent crustal movements, geoid and density distribution: Contribution from integrated satellite and terrestrial measurements, in *NRP 20—Deep Structure of the Swiss Alps*, edited by O. A. Pfiffner et al., pp. 25–259, Birkhäuser, Basel, Switzerland.

Kelsey, H. M. (1988), Formation of inner gorges, *Catena*, *15*, 433–458.

Knudsen, Ó., and P. M. Marren (2002), Sedimentation in a volcanically dammed valley, Brúarjökull, northeast Iceland, *Quat. Sci. Rev.*, *21*, 1677–1692.

Korup, O. (2006), Rock-slope failure and the river long profile, *Geology*, *34*, 45–48.

Kühni, A., and O. A. Pfiffner (2001), The relief of the Swiss Alps and adjacent areas and its relation to lithology and structure: Topographic analysis from a 250-m DEM, *Geomorphology*, *41*, 285–307.

Margielewski, W. (2006), Structural control and types of movement of rock mass in anisotropic rocks: Case studies in the Polish Flysch Carpathians, *Geomorphology*, *77*, 47–68.

Marinos, P., and E. Hoek (2001), Estimating the geotechnical properties of heterogeneous rock masses such as flysch, *Bull. Eng. Geol. Environ.*, *60*, 85–92.

McEwen, L. J., J. A. Matthews, R. A. Shakesby, and M. S. Berrisford (2002), Holocene gorge excavation linked to boulder fan formation and frost weathering in a Norwegian alpine periglaciofluvial system, *Arct. Antarct. Alp. Res.*, *34*, 346–358.

Meigs, A., W. C. Krugh, K. Davis, and G. Bank (2006), Ultra-rapid landscape response and sediment yield following glacier retreat, Icy Bay, southern Alaska, *Geomorphology*, *78*, 207–221.

Miller, J. R. (1999), The influence of bedrock geology on knickpoint development and channel-bed degradation along downcutting streams in south-central Indiana, *J. Geol.*, *99*, 591–605.

Mitchell, W. A., P. J. Taylor, and H. Osmaston (1999), Quaternary geology in Zanskar, NW Indian Himalaya: Evidence for restricted glaciation and proglacial topography, *J. Asian Earth Sci.*, *17*, 307–318.

Montgomery, D. R. (2001), Slope distributions, threshold hillslopes, and steady-state topography, *Am. J. Sci.*, *301*, 432–454.

Mudd, S. M., and D. J. Furbish (2005), Lateral migration of hillcrests in response to channel incision in soil-mantled landscapes, *J. Geophys. Res.*, *110*, F04026, doi:10.1029/2005JF000313.

Persaud, M., and O. A. Pfiffner (2004), Active deformation in the eastern Swiss Alps: Post-glacial faults, seismicity and surface uplift, *Tectonophysics*, *385*, 59–84.

Reusser, L. J., P. R. Bierman, M. J. Pavich, E. Zen, J. Larsen, and R. Finkel (2004), Rapid late Pleistocene incision of Atlantic passive-margin river gorges, *Science*, *305*, 499–502.

Rudoy, A. N. (2002), Glacier-dammed lakes and geological work of glacial superfloods in the Late Pleistocene, Southern Siberia, Altai Mountains, *Quat. Int.*, *87*, 119–140.

Safran, E. B., P. R. Bierman, R. Aalto, T. Dunne, K. X. Whipple, and M. Caffee (2005), Erosion rates driven by channel network incision in the Bolivian Andes, *Earth Surf. Processes Landforms*, *30*, 1007–1024.

Schlunegger, F., and M. Hinderer (2003), Pleistocene/Holocene climate change, re-establishment of fluvial drainage network and increase in relief in the Swiss Alps, *Terra Nova*, *15*, 88–95.

Schlunegger, F., and S. D. Willett (1999), Spatial and temporal variations in exhumation of the central Swiss Alps and implications for denudation mechanisms, *Geol. Soc. London Spec. Publ.*, *154*, 157–179.

Schlunegger, F., K. Detzner, and D. Olsson (2002), The evolution towards steady state erosion in a soil-mantled drainage basin: Semi-quantitative data from a transient landscape in the Swiss Alps, *Geomorphology*, *43*, 55–76.

Schmidt, K. M., and D. R. Montgomery (1995), Limits to relief, *Science*, *270*, 617–620.

Selby, M. J. (1992), *Hillslope Materials and Processes*, 2nd ed., 451 pp., Oxford Univ. Press, Oxford, U. K.

Shreve, R. L. (1972), Movement of water in glaciers, *J. Glaciol.*, *11*, 205–214.

Stock, G. M., R. S. Anderson, and R. C. Finkel (2005), Rates of erosion and topographic evolution of the Sierra Nevada, California, inferred from cosmogenic ^{26}Al and ^{10}Be concentrations, *Earth Surf. Processes Landforms*, *30*, 985–1006.

Tinkler, K., and E. Wohl (1998), A primer on bedrock channels, in *Rivers Over Rocks: Fluvial Processes in Bedrock Channels*, *Geophys. Monogr. Ser.*, vol. 107, edited by K. J. Tinkler and E. E. Wohl, pp. 1–18, AGU, Washington, D. C.

Tricart, J. (1960), A subglacial gorge: La Gorge du Guil (Hautes-Alpes), *J. Glaciol.*, *3*, 646–651.

Tucker, G. E., and R. L. Bras (1998), Hillslope processes, drainage density, and landscape morphology, *Water Resour. Res.*, *34*, 2751–2764.

Von Poschinger, A. (2005), Der Flimser Bergsturz als Staudamm, *Bull. Angew. Geol.*, *10*, 33–47.

Whipple, K. X., and G. E. Tucker (2002), Implications of sediment-flux-dependent river incision models for landscape evolution, *J. Geophys. Res.*, *107*(B2), 2039, doi:10.1029/2000JB000044.

Whipple, K. X., G. S. Hancock, and R. S. Anderson (2000), River incision into bedrock: Mechanics and relative efficacy of plucking, abrasion, and cavitation, *Geol. Soc. Am. Bull.*, *112*, 490–503.

Wyllie, D. C., and C. W. Mah (2004), *Rock Slope Engineering, Civil and Mining*, 4th ed., 431 pp., Spon Press, London.

Ziegler, H. J. (1982), Die Hangbewegungen im Lugnez, am Heinzeberg und bei Schuders (Graubünden), Geologie und Geomechanik, Ph.D. thesis, 106 pp., Geol. Inst., Univ. of Berne, Berne, Switzerland.

O. Korup, WSL/SLF, CH-7260 Davos, Switzerland. (korup@slf.ch)

F. Schlunegger, Institute of Geology, University of Berne, CH-3003 Berne, Switzerland.